ELSEVIER

Journal of Atmospheric and Solar-Terrestrial Physics 68 (2006) 1136–1160

Journal of ATMOSPHERIC AND SOLAR-TERRESTRIAL PHYSICS

www.elsevier.com/locate/jastp

Estimates of meteoroid kinetic energies from observations of infrasonic airwaves

Wayne N. Edwards[a,*], Peter G. Brown[b], Douglas O. ReVelle[c]

[a]*Department of Earth Sciences, University of Western Ontario, 1151 Richmond St., London, Ont., Canada N6A 5B7*
[b]*Canada Research Chair in Meteor Science, Department of Physics and Astronomy, University of Western Ontario, 1151 Richmond St., London, Ont., Canada N6A 3K7*
[c]*Atmospheric, Climate and Environmental Dynamics, Meteorological Modeling Team, P.O. Box 1663, MS D401, Los Alamos National Laboratory, Los Alamos, NM 87545, USA*

Received 1 November 2005; received in revised form 22 February 2006; accepted 25 February 2006
Available online 18 April 2006

Abstract

Signal properties of the acoustic waves produced from meteoroids impacting the Earth's atmosphere in the approximate size range of 0.1–10 m diameter have been analyzed at infrasonic frequencies. From these data, we have produced a series of empirical relations between the far-field acoustic signature of the bolide shocks and meteor source energies by correlating infrasonic observations of those fireballs which are also detected by earth-observing satellites. Adopting a similar approach as has been previously employed for man-made explosives, signal properties such as acoustic amplitude, signal energy/power and signal-to-noise ratio, are shown, after high-altitude wind corrections, to be useful tools in estimating the kinetic energy of a bolide. Comparison of bolide infrasound data to ground-based explosive tests show that the acoustic amplitudes from airwaves generated by small bolide events (<7 kt TNT equivalent) attenuate more rapidly than nuclear or chemical explosions. As well, acoustic amplitude values for bolides are systematically lower than acoustic amplitudes measured for equivalent ground-based explosions. This is interpreted to be largely due to bolide acoustic sources being at high altitudes in the atmosphere. We find from our analysis that these heights are on average located between 20 and 30 km. Larger events (>7 kt) mimic man-made explosions in terms of range dependence, but offset in amplitude equivalent to ~20 km source altitudes. This is consistent with instrumental observations of fireballs and the expectation that larger meteoroids (greater than a few meters in diameter), should penetrate deeper into the atmosphere on average. Applying these new relationships to historical events, we find that the August 3, 1963 bolide detected infrasonically near the Prince Edward Islands off the coast of South Africa, previously estimated to have an energy of 1100 kt, may have had a much smaller energy of 266 ± 90 kt. This energy revision brings the infrasonically determined Near Earth Object (NEO) influx rate into much better agreement with that determined more recently using satellite and telescopic survey data.

Keywords: Infrasound; Meteor; Fireball; Bolide; Kinetic energy; Acoustic waves

*Corresponding author. Tel.: +1 519 8502385; fax: +1 519 6612033.
E-mail address: wedwards@uwo.ca (W.N. Edwards).

1364-6826/$ - see front matter © 2006 Elsevier Ltd. All rights reserved.
doi:10.1016/j.jastp.2006.02.010

1. Introduction

Meteoroids encounter the Earth's atmosphere at velocities between 11 and 72 km/s. The kinetic energy carried by particles at these velocities is tens to hundreds of times the equivalent energy of an equal mass of high explosive. The sudden deposition of this energy during the disintegration and deceleration of large meteoroids produces a spectacular light show which may be visible for hundreds of kilometers. During this interaction with the Earth's atmosphere, the light, sound and ionization produced can be used to infer the original mass, orbit and other physical/chemical properties of the parent meteoroid. For larger meteoroids, some material may survive to reach the Earth's surface in the form of meteorites, providing one of the few opportunities by which samples of other regions of the solar system can be studied at the Earth.

Historically, visual/optical observations have been the staple for study of bright fireballs, with eyewitness accounts, photographic and video observations being the primary mode of data collection (Ceplecha et al., 1998). However, other observational techniques can also play an important role in defining the processes occurring during the brief period of meteoroid—atmosphere interaction. One such technique is infrasonic recordings of the acoustic signals produced when the original shock waves produced by the hypersonic passage of the meteoroid decay at large ranges from the fireball trajectory. This mode has been used infrequently in the past due to limited numbers of deployed detectors, but it is seeing increased usage in fireball studies as the International Monitoring System of the Comprehensive Nuclear Test Ban Treaty nears completion, a component of which is a global 60 station infrasound network.

Infrasound, the part of the acoustic spectrum lying below the range of human hearing and above the atmospheric Brunt–Vaisala frequency where gravity waves begin (approximately between the range of 20–0.001 Hz), is of particular interest due to the lack of significant attenuation at these frequencies in the Earth's atmosphere (Beer, 1974), allowing these acoustic waves to be observed even after traveling thousands of kilometres. Traditionally, it was the long observational range of infrasound which led to its adoption as the method of choice for monitoring of nuclear and large chemical explosions during the 1950s and 1960s before the advent of satellite detectors. Interest in infrasound waned, however, after the signing of the Tri-Lateral Limited Test Ban Treaty which banned atmospheric and undersea nuclear tests and forcing further tests to be held underground. This history has led to a legacy of terminology that is still in use in the infrasonic literature and observations. The most obvious of these in the following sections will be the use of the term "yield", meaning the total energy of the infrasonic wave source (in the present study, the initial kinetic energy of the meteoroid), and the use of kilotons of equivalent TNT (1 kt TNT $= 4.185 \times 10^{12}$ J) as a measure of this energy. Since the late 1990s infrasound has seen a rebirth, again as a monitoring tool, but now for verification and enforcement of the Comprehensive Nuclear Test Ban Treaty (Christie et al., 2001); however this global network of microbarometers is equally capable of listening to the impacts of large meteoroids on a global scale, a feature we exploit in the following study.

Large meteoroids, 0.1–10 m in diameter, are a natural, impulsive source of infrasonic waves at the Earth's surface, produced during the hypersonic passage and fragmentation phases of meteoroid flight. The most famous example is the Great Siberian Meteor of 1908. Occurring over the Tunguska River in southern Siberia on June 30, 1908, the infrasonic waves produced by the disintegration of the object were observed over most of Russia and Eastern Europe (Whipple, 1930, 1934, Astapowitsch, 1933, 1934). Meteors can produce infrasound by two mechanisms (1) the hypersonic shock of the meteor's passage through the atmosphere and (2) fragmentation of the meteoroid itself, which leads to efficient coupling to the atmosphere and a sudden increase in the fraction of total energy channeled into shock production. The degree to which either mechanism dominates infrasound production over the other varies from event to event. Since the early work of ReVelle (1976) and more recently Brown et al. (2002a–c, 2004), enough additional bolide infrasonic signals have been well observed by this network to begin to look at bolide infrasound in a statistical way. The goals of the present study are to use a large database of bolide infrasound observations with the following specific aims:

1. Examine infrasonic signal properties statistically as a function of range, atmospheric winds and bolide yield (as derived by satellite observations) to derive empirical relations between source energy and these infrasound signal metrics.

2. Compare the source energies measured with these empirical relations to previous (mainly theoretical) estimates of bolide energies
3. Apply these new relations to several major historical bolide infrasound events.

We begin by reviewing previous techniques used to estimate bolide source energy from infrasound observations. Next we define the methods used to identify fireball airwaves in infrasound data, the specific signal processing and analysis methodology we have employed and our expectations of the form of the empirical relations from theoretical considerations. Finally, we compare our relations to those found from high explosive and nuclear tests, apply our results to the Revelstoke, Kincardine and the African Prince Edward Islands fireballs to make new estimates for their yields and compare our energy estimates to those from other techniques.

2. Previous methods of energy determination using infrasound

Prior to the work presented here, kinetic energy estimates for bolides using infrasound have been accomplished through both theoretical methods and previously determined empirical calibration curves originally produced from man-made ground-level atmospheric explosions. The first theoretical treatment of the production, propagation and attenuation of meteor infrasound was presented by ReVelle (1974, 1976). Extensions of this early work have led to several methods of energy estimation using weak shock propagation theory. Valid in the weak shock regime, using observed acoustic wave period and amplitude for line sources (Ceplecha et al., 1998) leads to

$$E_S = 11.5\pi\rho_m R'^3 \left(\frac{\Delta p}{\sqrt{p_S p_g}}\right)^4 \frac{c_S^3}{V}, \quad (1)$$

where the variables are defined below. Equivalently, the wave period method for line sources, where linear propagation is assumed at great range after an initial weak shock phase (Ceplecha et al., 1998) produces

$$E_S = \frac{\pi}{12}\rho_m \left(\frac{\tau}{1.579}\right)^4 \frac{c_S^7}{V} R'^{-1}, \quad (2)$$

while the acoustic efficiency method for ducted point and line sources (ReVelle and Whitaker, 1995) produces

$$E_S = \frac{2\pi R^2 E_{aw}}{\varepsilon_{ac}} \left(\frac{1-f_R}{1+f_R}\right) f_R^{-n},$$

where

$$n = R/R_{max}, \quad (3)$$

where E_S is the bolide source energy (J), E_{aw} the observed acoustic wave energy per unit area at the observation point (J/m^2); ρ_m the density of the meteor (kg/m^3); Δp the observed signal overpressure (Pa); p_g the ambient pressure at the ground (Pa); p_S the ambient pressure at the source altitude (Pa); c_S the average acoustic sound speed (m/s); V the meteor velocity (m/s); τ the observed period of signal at maximum amplitude (s); ε_{ac} the acoustic efficiency; f_R the ground reflection factor of Cox (1958); R' the slant range between source and receiver (m); R the ground projected range to source (m); R_{max} the ducted wave skip distance, counterwind (200 km), downwind (400 km) (m).

A similar detailed analytical treatment of meteor infrasound was also attempted by Golitsyn et al. (1977) and recently applied to infrasonic observations of the Vitim bolide by Shumilov et al. (2003). Here the overpressure of the wave was found to vary as

$$\Delta p = \frac{(\gamma-1)E_S(R'-c_S t)\exp\{-(z/2H)-(c_S t-R')^2/(a^2\sin^2\theta+L^2\cos^2\theta)\}}{2\pi^{3/2}R'(a^2\sin^2\theta+L^2\cos^2\theta)^{3/2}}, \quad (4)$$

where the remaining undefined quantities are as follows: γ is the ratio of specific heat at constant pressure and constant volume (diatomic gas $\gamma = 1.4$), t the time (s), z the observation altitude (m), H the scale height of the atmosphere (m), a the source's characteristic dimension (i.e. width) (m), L the length of the meteor trail (m), θ the observation angle as measured from the trajectory plane (radians).

Despite its complexity and the enormous effort which has gone into its development, in practice we find the Golitsyn et al. (1977) expression works poorly as a source energy estimator for the events

we have examined as the wave periods it predicts are generally far larger than observations show.

Unfortunately a common issue with all these theoretical methods is that they contain variables which are often unknown for a specific event, such as the meteoroid density, velocity, source altitude, trail length and acoustic efficiency. In practice, these values are usually given observed averages or simply assume average values. These theoretical approaches are only really effective when a bolide has a well-observed trajectory and velocity and has recovered meteorites, a situation rarely achieved.

As an alternative method to these theoretical treatments, bolide infrasound observations have been combined with empirical calibration curves of range–yield–amplitude (or period) derived from man-made nuclear and chemical explosives based on many observations. It has not been clear how robust these empirical fits would be to bolides; however, the impulsive nature of the two types of sources should provide at the very least order of magnitude correct energy estimates for bolides.

The most commonly used of all empirical energy estimators have been those produced by the US Air Force Technical Applications Centre (AFTAC). The first of these relates the observed period of the signal during maximum amplitude to the source energy:

$$\log(E_S/2) = 3.34\log(P) - 2.58, \quad E_S/2 \leqslant 100\,\text{kt}, \tag{5a}$$

$$\log(E_S/2) = 4.14\log(P) - 3.61, \quad E_S/2 \geqslant 40\,\text{kt}, \tag{5b}$$

where P is the period at maximum amplitude for the signal in seconds and the source yield, E_S, is the measured in kt of TNT (Ceplecha et al., 1998). It has been argued this relationship between period and energy is a fundamental property of point and line source explosions (ReVelle, 1976), however, as will be seen (Section 7) this argument is not without its problems. Note the factor of 1/2 in the energy estimates results from the original expressions being derived for nuclear explosions, where approximately 50% of the initial energy is carried away by radiation (Glasstone and Dolan, 1977) and thus not available for shock production.

The second empirical energy estimator, again produced by AFTAC, relates observed infrasonic peak amplitudes (in Pa), P, from nuclear weapons tests, to source energy (Clauter and Blandford, 1998):

$$\log E_S = 2\log P + 2.94\log \Delta - 1.84, \tag{6}$$

where Δ is the range from source to receiver in degrees. Similar relationships have been found by others and been used to estimate bolide kinetic energies. For example, based on French nuclear weapons test observations a similar curve to that of the AFTAC amplitude curve was found (Blanc et al., 1997):

$$\log E_S = 2\log P + 3.52\log R - 10.62. \tag{7}$$

Noting that despite both these calibrations using many observations of nuclear explosives with known source energies at known distances, the variation within the observations can be significant, as seen when comparing the two calibrations side by side (Fig. 1).

Using more conventional chemical explosives, ammonium nitrate fuel oil (ANFO), Davidson and Whitaker (1992) found that for the Miser's Gold Test the infrasonic observations best fit a curve of the form:

$$\log E_S = 1.55\log P_c + 2\log R - 8.45. \tag{8}$$

While some time later using a data set containing a wider variety of ANFO yields as observed by the Los Alamos National Labs' infrasound network, Whitaker (1995) found that more generally

$$\log E_S = 1.47\log P_c + 2\log R - 4.96, \tag{9}$$

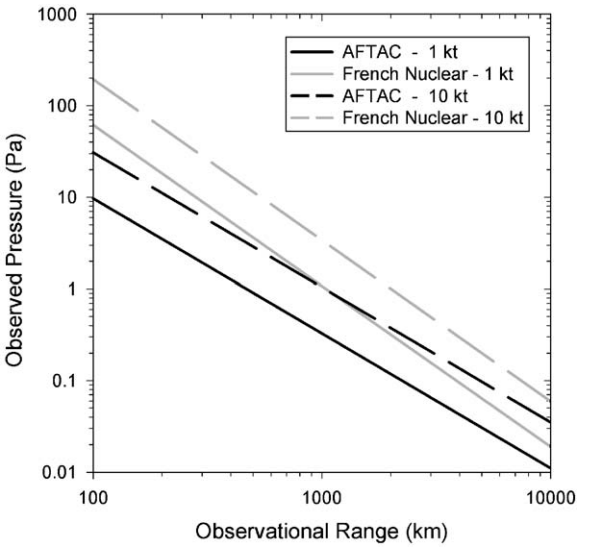

Fig. 1. Comparison of Infrasound–Source Energy calibrations for nuclear explosions as determined by the United States Air Force Technical Applications Centre (AFTAC) (Clauter and Blandford, 1998) and from French nuclear tests (Blanc et al., 1997).

where P_c is wind corrected amplitude (Davidson and Whitaker, 1992) (discussed later in Section 6). All pressure amplitudes for these calibrations (Eqs. (6)–(9)) are measured in Pascals, ground range, R, in kilometres and source energy, E_S, in kilotons of TNT equivalent explosive energy. We will compare these earlier relations to our final empirical yield estimations to establish the range of expected yields for given amplitude–range combinations.

3. Fireball acoustic signal identification and details of the data set

The combination of space-based sensors, operated by the US Department of Defense (DoD) and Department of Energy (DoE), recordings' of fireballs and the growth of the global infrasound network portion of the International Monitoring System (IMS) (operated by the Comprehensive Nuclear Test Ban Treaty Organization (CTBTO) since the late 1990s) have proven to be excellent complementary tools for globally identifying bolide infrasonic airwaves. Space-based optical and infrared observations of bolide explosions in the atmosphere not only provide both a tool for identifying the location and time of the source, but also an independent estimate of the explosive yield of the event using the relation between optical energy and the total energy of the event (Tagliaferri et al., 1994; Brown et al., 2002a). The source yields, determined from optical sensors, are somewhat uncertain; the energies derived assume the bolides radiate as 6000 K blackbodies, an approximation at best. However, the values measured using this assumption have proven remarkably close to energy estimates found independently from other techniques and ground-truthed events where meteorites have been recovered (and for which initial masses are known with greater precision than is typically the case). Table 1 compares several specific cases where satellite optical yields have been measured and energies from techniques other than infrasound and/or meteorites are available. Although the agreement with yield in these cases is quite good (all agree within error), we caution that events with unusual composition/porosity, such as might be expected from cometary sources or from iron meteoroids, would be expected to have atypical radiation efficiencies (ReVelle, 2005). Nevertheless, the level of agreement between satellite data and the four ground-truthed events (all chondritic "normal" fireballs) suggests that for most cases the accuracy of the satellite energy estimations should be better than 20–30%.

Once satellite geographic locations for a bolide are obtained, it becomes a straight forward task to determine the estimated arrival time window for any infrasonic waves associated with the event, assuming average signal propagation velocities from 0.285 to 0.310 km/s stratospheric arrivals) and 0.260–0.220 km/s (thermospheric arrivals) (cf. Ceplecha et al. (1998) for a complete description of expected infrasonic arrival modes). Here the average propagation velocity of an infrasonic wave is defined as the great circle distance separating source and receiver divided by the total time required for the wave to travel this distance. In addition, the direction from which a signal may be expected to arrive is also determined. Signals arriving at a microbarometer array within the estimated arrival

Table 1
Initial velocity, initial mass and total energy estimates for six recent well-observed fireballs which produced meteorites and comparison to satellite yield estimates for events where satellite observations are available

Meteorite fall name	Initial velocity (km/s)	Initial mass (kg)	Bolide energy best estimate (kt)	Satellite observed energy (kt)	Reference
Villalbeto de la Peña	17±1	750±150	0.026±0.006	—	Llorca et al. (2005)
Park Forest	19.5±0.3	11000±3000[a]	0.50±0.14	0.41±0.11	Brown et al. (2004)
Neuschwanstein	20.95±0.04	500±200	0.026±0.011	—	Spurny et al. (2003), ReVelle et al. (2004)
Moravka	22.5±0.3	1500±500	0.091±0.030	0.089±0.034	Borovička et al. (2003)
Tagish Lake	15.8±0.5	70300±8300	2.10±0.28	2.53±0.27	Brown et al. (2002c)
St. Robert	13.0±0.3	1750±250	0.035±0.005	0.050±0.022	Brown et al. (1996)

All satellite-measured energies are determined via Eqs. (10) and (11) using the original published optical energy observations.
Note: Satellite energies derived assuming a 6000 K blackbody.
[a]Average/std. error of all stated initial mass estimates.

window and with back azimuths at or near the expected direction, can, with a high degree of certainty, be associated with the observed satellite observation. The signal processing methods and general techniques for infrasound array angle of arrival measurements are described in Evers and Haak (2003) and Brown et al. (2002b).

All of the bolide events used in the following study were observed both by optical and infrared space-based sensors operated by the DoD and DoE and have a minimum of one infrasonic, or microbarograph array detection. The data set currently includes 31 separate bolide events, with 64 individual observations by various infrasound arrays located worldwide. The bolide locations also range worldwide with events located over the Pacific and Indian oceans and every continent including Antarctica and the European sub-continent. In general, most infrasonic observations in the data set (~80%) are concentrated between the ranges of 1500–5500 km, although outliers include observations at closer ranges of ~300 km and extremely distant observations at ranges greater then 9000 km (Fig. 2). All infrasonic observations with ranges less than 250 km, roughly corresponding to the minimum range required to observe a stratospherically ducted wave, were removed from the data set. Additionally all observations with average propagation velocities less then 0.260 km/s were removed (as these may have been thermospheric returns), along with a single anomalous observation (Fig. 3a,b), hence the final data set is composed exclusively of the most commonly observed infrasonic waves; stratospherically ducted arrivals. Statistics of the average wave propagation speed confirm this with an average signal velocity for all observations of 0.302 ± 0.017 km/s, which is expected to be almost solely composed of stratospherically ducted signals (Ceplecha et al., 1998). The observed scatter amongst the stratospheric propagation velocities (Fig. 3a/b) is in part due the anisotropic effects due

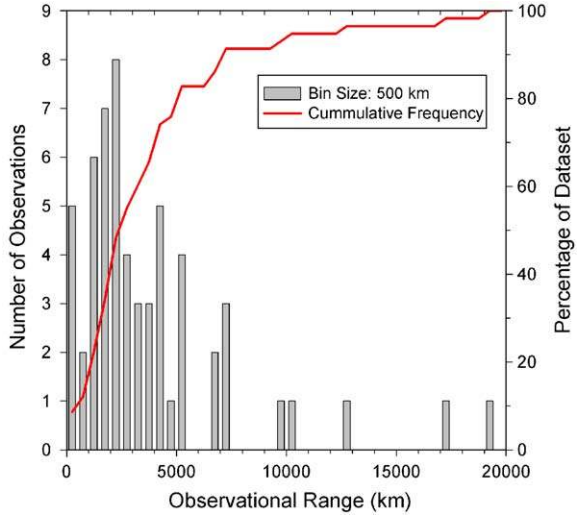

Fig. 2. Histogram and cumulative frequency plot of the observational ranges for the entire bolide infrasound database.

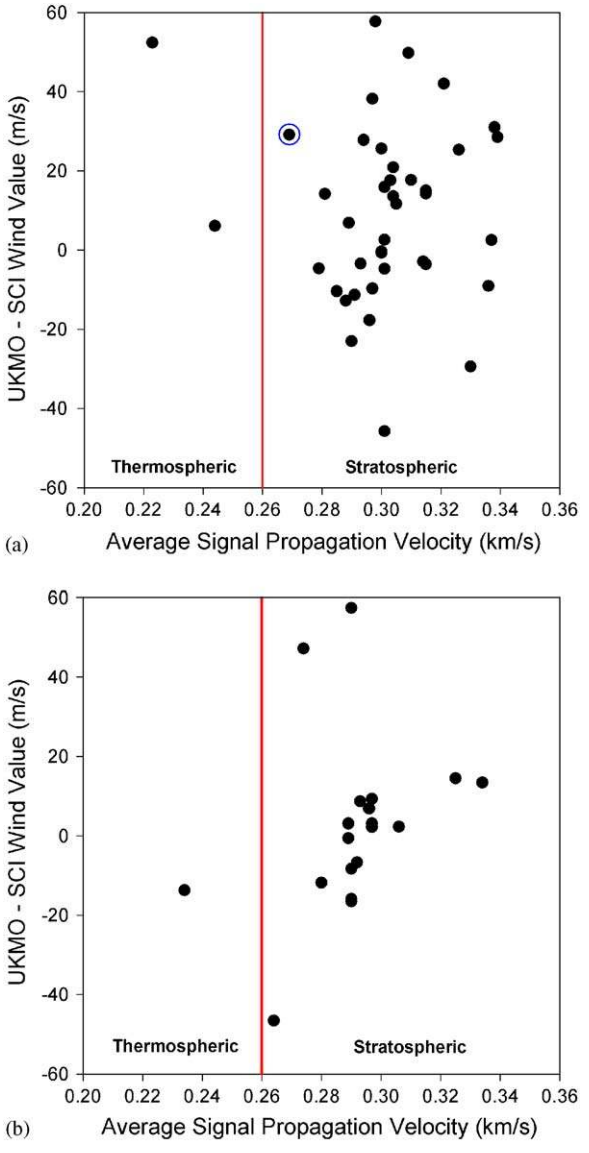

Fig. 3. Average signal velocity cutoff distinguishing between observed thermospheric and stratospheric ducted acoustic waves for (a) small bolides (<7 kt) and (b) large bolides (>7 kt). *Note*: The circled small bolide observation was also removed due to an unexplained and unusual 180° rotation of the observed back azimuth relative to the expected azimuth.

to the presence of high-altitude winds; increasing velocity downwind, decreasing upwind. Correction of measurements for wind effects and the significance of the UKMO-SCI index, a measure of the strength and direction of these winds, are discussed in detail later in Section 6. Although portions of some signals may include some thermospheric components, these contributions are thought to provide minimal contamination, due to the large dispersion and absorption of a wave propagating over the range of heights of a thermospheric path.

Lastly, the bolide events that meet the qualifications outlined above are then separated into two groups, "large" events are defined here as those whose estimated source energies are greater than 7 kt and "small" events, with source energies below 7 kt. This step, suggested previously by Edwards et al. (2005), is an attempt to test the hypothesis that larger, more energetic bolides should penetrate deeper into the atmosphere and thus deposit acoustic energy lower in the atmosphere than smaller bolides. The separation of these two groups has been made possible by recent detections of very energetic bolides by several IMS infrasound arrays (Klekociuk et al., 2005). The choice of using the seemingly arbitrary 7 kt as the cutoff for these two groups comes from a natural gap in our bolide infrasound database near this energy. Currently there are no events with satellite estimated source energies between 5 and 7 kt.

4. Data processing methodology

To ensure that no systematic biases were introduced in the processing of detected airwave signals, a homogenous process was developed and automatically applied to all raw bolide airwave signals.

After an infrasonic signal from a bolide was identified, a series of pre-processing steps were taken before signal measurements were made. These steps remained unchanged for most of the detected signals, save for those few events which warranted an increase to the bandpass width due to large estimated yields (as deduced from satellite observations and the raw waveforms) or the presence of signal energy at higher frequencies seen in spectrograms of the raw waveforms due to the relative proximity of the infrasound station to the source bolide. Typically, bandpass adjustments for very large events required a slight lowering to the lower cutoff frequency, while those stations closer to the source required an increase to the upper cutoff frequency to include energies in the signal at higher frequencies ensuring that all the signal energy was covered in the chosen bandpass. Numerical tests involving variations in the bandpasses for most events outside the nominal range produced negligible differences in the final results (except for the cases just mentioned).

Once preprocessing was completed, various measurements of the properties of each signal were made. The precise steps in this reduction methodology are outlined in detail to allow other researchers to reconstruct our results from the raw digital data and to allow comparison with future airwave bolide measurements. These data were processed using the analysis package MatSeis 1.7 (Harris and Young, 1997, Young et al., 2002) (available from http://www.nemre.nnsa.doe.gov/cgi-bin/prod/nemre/matseis.cgi).

Step 0: Instrument response correction for large events

The initial step of correcting for the response of the instrument (typically composed of a microbarometer and digitizer) is particularly important for very energetic events where significant components of the signal spectrum may be at very low frequencies. Currently, the two most commonly used microbarometers (MB2000 & Chaparral 5) have responses which begin to roll off in sensitivity at ~0.05 Hz. This loss of sensitivity is approximately −5 dB between 0.05 and 0.01 Hz for the Chaparral 5 sensor and −3 dB for the MB2000 sensor in the same frequency range. Correcting for this sensitivity loss ensures that the bolide signal content is as complete as possible for each event. Thus, in our study, before any measurement is made, each infrasound channel has the instrument response above 0.01 Hz (provided by the CTBTO for each station) applied to the signal. This provides a best estimate of the original atmospheric waveform independent of the instrument.

Step 1: Onset and duration of the signal

This step is an extension of the identification method already discussed. The signal onset (or arrival time) was determined by the start of a constant azimuth, (defined as settling to within a consistent value within 10° over 5 windows), from the generally random azimuths of typical background noise. For extremely short ranges (less then a few 100 km) this azimuth will often vary greatly (depending on orientation) as a bolide moves across the sky. Such close range observations are removed from the data set through the requirement that the signal be truly stratospherically ducted and hence at

least one "skip" distance separate source and receiver. For the remaining signals typically occurring at ranges of many 100s–1000s of kilometres distance, often very little variation in back azimuth is seen as the moving-source better approximates a point-source. Similarly, the end of the signal (and thus its duration) was determined by the return of the computed azimuths from an approximately constant value to that of the random noise. In cases where this azimuth change may be ambiguous, the element pairwise cross correlation maximum and/or the Fisher *F*-statistic (Melton and Bailey 1957) were used as guides to the onset and duration of the signal.

Step 2: Average signal azimuth and trace velocity

Signal averages for back-azimuth and trace velocity were calculated for each signal over the entire duration of the signal as defined in step 1, using the computed azimuths and velocities from the cross correlation procedure. These two values were then taken to define a single velocity vector for the entire incoming wave, which we assume is a plane wave, over the size-scale of the infrasound array. An example of this process is shown in Fig. 4.

Step 3: Waveform stacking

Using the average back-azimuth and trace velocity, delay times to the onset of the signal were calculated for each element in the particular array, relative to the prime array element or the average element position. These delay times were then used to shift and phase align each element's observed waveform, again assuming the signal propagated across the array as a plane wave. After phase alignment, the array elements were then stacked to produce an "optimum" waveform, (often referred to as the best beam), with the result that incoherent noise should be reduced by a theoretical factor of $1/\sqrt{N}$, where N is the number of array elements stacked.

Step 4: Maximum signal envelope amplitude

To pick the maximum amplitude of the signal envelope, the stacked, raw waveform is first bandpass filtered using a second-order Butterworth filter with corner frequencies of 0.2 and 3.0 Hz, except in circumstances mentioned previously. Once filtered, the waveform's amplitude envelope is then computed using the Hilbert Transform (Dziewonski and Hales, 1972). The peak of the envelope is taken as the maximum amplitude of the signal.

Step 5: Peak-to-peak amplitude and the period at maximum amplitude

The more common method of amplitude measurement, used when dealing with atmospheric explosions (e.g. nuclear free air bursts), is the maximum peak to trough distance of the waveform. This was measured within the time pick of the previously found envelope maximum. Additionally, the times of four zero-crossings about the peak amplitudes were taken and used to compute the period of the signal during the signal maximum. This method of period determination was used in order to maintain consistency with the methodology employed to construct the empirical period–energy relationships (Eqs. (5a) and (5b)) by AFTAC. This relation has been found to provide a reliable method to determine explosive yields for larger (i.e. nuclear) explosions (ReVelle, 1997).

Step 6: Total integrated signal energy/power and background noise levels

Estimates of the observed signal's total energy (or power) content were determined by squaring and then summing each sample of the filtered, optimum waveform (best beam) over the entire duration of the signal. A similar procedure was also performed for the stacked and filtered measurements, of equal duration, taken prior to the onset of the signal and after the signal had ended. Here the assumption is made that the ambient noise levels have remained constant throughout the duration of the signal. This may not be an entirely valid assumption for long duration signals at all observation sites. These values were then averaged to evaluate the energy associated with the ambient background noise. This background noise energy was then subtracted from the raw signal energy to obtain an estimate of the total amount of energy due solely to the bolide airwave at the observation site (Brown et al., 2002b).

Step 7: Integrated energy signal-to-noise ratio

Finally, in an attempt to account for the varying background noise levels at each array site, which may contaminate simple amplitude measurements, an estimate of the signal-to-noise ratio for the duration of each observed signal is made. This is achieved using the raw integrated signal energy/power and the average background energy/power, values found in Step 6.

5. Bolide yields and scaling laws

Bolide yield, or equivalently the initial kinetic energy of a bolide, is calculated for each event using the total radiated optical energy observed by satellite and the radiation efficiency of Brown et al. (2002a):

$$\tau_I = 0.1212\, E_{\mathrm{Opt}}^{0.115}, \tag{10}$$

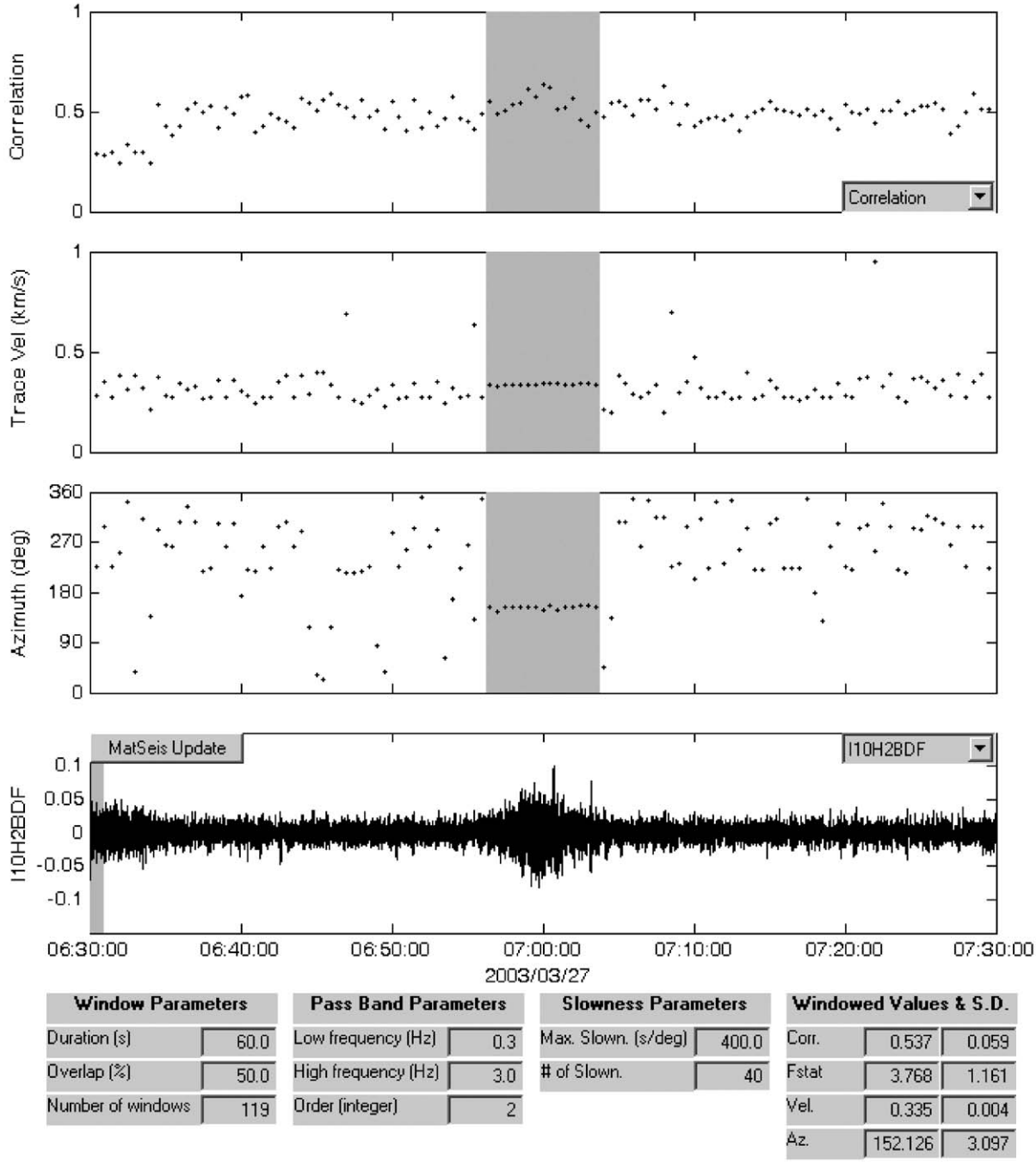

Fig. 4. Example of signal duration and average azimuth/trace velocity procedure using the observed signal at I10CA for the Park Forest fireball on March 27, 2003 and the Infra Tool analysis package of MatSeis (Young et al., 2002). Windows (top to bottom) show: correlation, trace velocity, back azimuth and the filtered waveform (in Pascals) of array element H1 (0.3–3.0 Hz). Shaded region is the approximately constant azimuth/trace velocity which marks the onset of the observed bolide signal as well as its duration. Azimuth and trace velocity values within this region are averaged; in this case 152.1° and 0.335 km/s, respectively.

where τ_I is the radiation efficiency and E_{Opt} is the observed radiation energy in the space-based sensor silicon-bandpass (cf. Tagliaferri et al., 1994) in kilotons of TNT equivalent ($1\,\mathrm{kt} = 4.185 \times 10^{12}\,\mathrm{J}$). Note that this relationship is quasi-independent as it used the AFTAC period relationship (Eqs. (5a) and

(5b)) in part as one method of energy determination. Although it will be shown that the AFTAC period–energy relation is more uncertain for energy estimates of small events (less then ~0.2 kt) and very large events (>10 kt), it appears to be a robust energy indicator for modest energy bolides of order ~1 kt. Fortunately, at smaller energies the radiation efficiency calibration is well supplemented with higher precision events which were given more weight, thus we believe Eq. (10) should remain a robust means of energy measurement. Once the radiation efficiency is known, the total bolide yield may be calculated directly from the satellite observed energy by the ratio:

$$E_S = E_{Opt}/\tau_I, \tag{11}$$

where E_S is bolide yield in kilotons of TNT equivalent. The radiation yield assumes spectral emission equivalent to a 6000 K blackbody (cf. Tagliaferri et al., 1994; Brown et al., 2004). Note that this empirical relation is very similar to that expected on theoretical grounds for H-chondrite-type meteoroids.

Once the bolide yield is known, comparisons between multi-station infrasonic observations of a single event may be made. However, to compare between multiple events, the laws governing how infrasonic wave amplitude increases with source energy must be known. Here we make the assumption that the signals detected originated from a point source. This approximation is valid in the case where a terminal detonation is a major feature of the ablation profile and/or when the observation range is large compared to the length of the bolide's trail. Since our source–receiver range is always >250 km (and typically >1000 km) and fireball path lengths rarely exceed 200 km, this approximation is almost always satisfactory. From this assumption, we next adopt the scaling laws discovered during the early work with nuclear free air explosions during the 1950s and 1960s where it was observed that range and yield were related by the ratio:

$$\frac{R}{R_0} = \left(\frac{E_S}{E_0}\right)^{1/3}, \tag{12}$$

where R_0 and E_0 are the reference range and yield (Glasstone, 1964). This expression physically scales each energy to a reference yield (1 kt)—the larger the yield the further away the receiver needs to be to detect an equivalent overpressure. A more complete version of this scaling law, as is relates specifically to the overpressure (amplitude) of an infrasonic wave, is given by ReVelle and Whitaker (1997)

$$\Delta p = C\left(\frac{p_0}{p}\right)^{(q-3)/3} R^{-q} E_S^{q/3}, \tag{13}$$

where C is a constant, p_0/p is the ratio of atmospheric pressures at the source and observation altitudes and $q = 1$ in the linear far-field acoustic regime, $1.1 \leqslant q \leqslant 2$ in the intermediate field and $q = 3$ in the near field. Without further information for each event concerning the equivalent height of the bolide at the time of its detonation height/range of primary energy deposition, we treat the first two terms as constants (regaining Eq. (12)) and scale the known range by the observed optical yield to produce a scaled range which should ideally be independent of a bolide's energy:

$$R_S = \frac{R}{E_S^{1/3}}, \tag{14}$$

where R is in kilometers and E_S is in tons of TNT equivalent energy (note yield here is not expressed in kilotons as a majority of observed bolides have energies of only a fraction of a kiloton).

This proportionality between yield and range is a result of the physical geometry of point source explosions. Within the immediate region surrounding the source, there exists a zone where the initial wave propagation is highly nonlinear (shockwaves). To describe the dimensions of this zone, consider a point source located at an altitude with a pressure, p_0. After detonation the source energy, E_S, becomes distributed over a sphere of radius, R_B, where

$$R_B = \left(\frac{E_S}{(4/3)\pi p_0}\right)^{1/3}. \tag{15}$$

This is often described as the blast radius of the explosion. Within this zone, propagation of the overpressure is as a highly nonlinear shock, while outside of this radius the overpressure continues to propagate but instead as a weakly nonlinear shock. Physically, this is the region where the energy density in the explosion is greater than the ambient atmospheric thermal energy density. Eventually, after some distance, this weakly nonlinear wave will also decay into a linearly propagating wave. Here it is observed that the blast radius, by virtue of a point source's spherical symmetry, is proportional to the cube root of the source energy or yield. Since quantities such as the initial overpressure and the fundamental period of the wave depend upon R_B,

the scaling factor of yield to the 1/3 power will tend to appear in the observations of point source-like explosions.

For bolides, the majority of the meteoroids acoustic energy is radiated over a short section near the end of the luminous trajectory where atmospheric penetration is deepest (cf. ReVelle, 2005). Viewed from large distances, (as is the case for most of the infrasonically observed bolides), this short section approximates a point source. However, it is noted that both the point source and cylindrical line source approximations make the additional assumption that the blast radius is small when compared to the scale height of the atmosphere (~7 km). When the blast radii begin to exceed this limit the spherical symmetry of the point source is lost and the aforementioned relationship begins to break down as internal gravity waves begin to dominate the atmosphere's response to the deposition of the source energy. For all bolides in our sample this assumption does not pose a problem as gravity waves are not the dominant type of observed wave, the bolide energies being well below the range where gravity waves would become important (cf. ReVelle, 1976).

6. Results: infrasound observations of bolides

Upon plotting the four measured signal properties for each fireball airwave, namely maximum signal envelope amplitude, peak-to-peak amplitude, total integrated signal energy/power and integrated signal-to-noise ratio as a function of scaled range, two notable features of the data were immediately obvious; the first was that all four measures, for both large and small events appear to be related to scaled range in a power-law-type distribution. The apparent linearity in log–log space appears to confirm the initial theoretical assumption of using an $E_S^{1/3}$ scaling law, although given the scatter of these data a similar observation is made using $E_S^{1/2}$ scaling. In accordance with a power law distribution, a regression equation for all measurements is chosen to be of the form:

$$A = 10^a R_S^b, \tag{16}$$

where A is the amplitude of the measurement, R_S, is scaled range, and a and b are the constants to be fit.

Comparing this regression equation to Eq. (13) with $q = 1$:

$$\Delta p = C\left(\frac{p_0}{p}\right)^{-2/3}\left(\frac{R}{E_S^{1/3}}\right)^{-1} \tag{17}$$

and a rearranged version of the line source weak shock propagation model (Ceplecha et al., 1998, Eq. (1)):

$$\Delta p = \left(\frac{V(p_z p_g)^{1/2}}{11.5\pi\rho_m c_S^3}\right)^{1/4}\left(\frac{R}{E_S^{1/3}}\right)^{-3/4}, \tag{18}$$

it is seen that all three Eqs. (16)–(18) show a similar power law dependence; the amplitude is equal to an effectively constant term which decays by some exponent of scaled range. Thus a power law fit to the observations is justifiable on both observational and theoretical bases.

The second observation, seen in the raw observations, is that these data show significant scatter, particularly for small events <7 kt. This is reflected in their fitted R^2 values which range between 0.262 and 0.352 for small events and 0.339 and 0.741 for large events. Here R^2 (calculated in log–log space) is the commonly used estimator of the variance in the data and the quality of a linear regression and is defined as

$$R^2 = \left(\frac{\sum(x_i - \bar{x})(y_i - \bar{y})}{N\sigma_x\sigma_y}\right)^2, \tag{19}$$

where x_i, $\bar{x}$ and σ_x are the values, mean and standard deviation of the scaled range observations, respectively (similar for the amplitudes, y) and is equivalent to the square of the data correlation. If a usable relation to deduce bolide source energy (yield) from infrasonic observations is to be found, the observational scatter must be reduced. Note that we use R^2 as a first-order goodness of fit and are ignoring the uncertainty in both x and y variables.

Reducing the scatter in scaled range requires primarily a reduction in error in satellite deduced yield (since the error in physical range is negligible by comparison), which itself requires reduction of scatter in the luminous efficiency calibration (Eq. (10)). This may only be fulfilled by increasing the number of observed bolides with well-determined energies. As time is the primary factor required to achieve this goal, scatter in scaled range may be viewed as currently irreducible, until enough new, highly calibrated fireball-meteorite events observed by satellite can be obtained. However, scatter along the amplitude axes may be reduced more easily through an estimate of the directional effects of atmospheric winds. We expect the amplitude scatter in the raw observations reflect variations in (a) the wind conditions along each of the different source—receiver paths, (b) variations

in the height of primary energy deposition for each event as well as (c) differences in nonlinear losses for each event. Only the first of these mechanisms can be taken into account meaningfully for each event; the other two need to be estimated statistically or from numerical modeling.

At upper stratospheric altitudes of approximately 30–60 km, the Earth's wind profile reaches a local peak, with winds reaching speeds up to 100 m/s. These winds occur from generally easterly directions during the summer months and reverse to more westerly winds during winter months in the Northern hemisphere and in the opposite sense in the Southern hemisphere (Webb, 1966). These high winds are appreciable when compared with the local ambient sound speeds (~300 m/s) and produce a directional anisotropy in the acoustic velocity field that tends to focus acoustic wave energy when propagation is along downwind directions, while at the same time inhibiting propagation upwind. The observational result of this effect is that acoustic signals propagating along downwind directions show systematically larger amplitudes and are observed at more distant ranges than are those moving in upwind directions. Observations of this effect are documented mainly for man-made explosive sources (e.g. Davidson and Whitaker, 1992), but are expected to be just as common for natural sources, such as bolides.

To correct for this amplitude altering effect we introduce a similar correction method introduced by Mutschlecner and Whitaker (1990), used previously by Davidson and Whitaker (1992) for the Miser's Gold high explosive test and by Stevens et al. (2002) for analysis of nuclear tests undertaken by the former Soviet Union. The method uses a wind correction of the form:

$$A_{\mathrm{W}} = 10^{k v_{\mathrm{h}}} A, \tag{20}$$

where A is the measured quantity to be corrected, v_{h} is the horizontal component of the wind vector directed toward the receiver in metres/second and k is an empirical constant in seconds per meter. In a slight modification to the scheme of Mutschlecner and Whitaker, who used the wind component of the Stratospheric Circulation Index (Webb, 1966), we have used an average of the mean wind component directed toward the observation between 40 and 60 km altitude as measured by the Upper Atmosphere Research Satellite (UARS) and assimilated into daily global wind maps by the United Kingdom Meteorological Office (UKMO) (Swinbank and O'Neill, 1994). By using UKMO wind data as opposed to strictly modeled numbers, such as the Naval Labs Horizontal Wind Model (Hedin et al., 1996) used previously by Edwards et al. (2005), we believe the best possible estimate for the actual winds present at the time of an event are being used, as opposed to using average global winds.

Using the assimilated UKMO data at steps of 125 km in range (half the minimum allowed range in our study) along the great circle path connecting source and receiver, the wind components along the source to receiver direction are computed at and between standard pressure intervals given by

$$p_i = 1000 \times 10^{-i/6}, \tag{21}$$

where $i = 1,2,3 \ \ldots \ n$ and p_i is in units of hPa or mbars. Wind components at levels corresponding to between 40 and 60 km altitude (~2.5 and 0.3 hPa) are then averaged. These mean wind components are then further averaged again along the entire great circle path. This process is repeated for each event, providing an average wind value along the propagation path length for each observation. Using this method, local seasonal and global variations in stratospheric winds are all included in the final horizontal wind correction component, v_{h}.

The magnitude of the wind correction, determined by the value k, was found by iteration over a wide range of potential values from -0.1 to $+0.1$. For each trial value of k, all observations were scaled by Eq. (20) and a least-squares solution found; next the R^2 value of the new regression was computed and compared until a peak in the R^2 value was identified (Fig. 5a/b). The value of k at this peak, as well as the parameters of the least-squares regression were then taken to be the bolide infrasound calibration curves. The correction for stratospheric winds improves scatter along the regressed fit significantly for the small event data set, increasing R^2 values from 24% (signal-to-noise ratio) to 68% (peak-to-peak amplitude), while for the large bolide event data set very little improvement was seen (0.1–1%). This apparent insensitivity to the effects of winds for the large bolide data is likely the result of a particular bias in the observations for these events. For most of the (small number) of large bolide observations, average wind values are small to moderate as a result of either the weather conditions at the time of the event or nearly meridonal propagation paths, cutting across the primarily zonal stratospheric wind flow. Since

observations in the large bolide data set lack the variety of possible orientations present in the small bolide observations, the scatter associated with winds is not as prevalent; this results in the best-fits being at small k values.

Comparison of the peak-to-peak amplitude correction factor for small bolide data ($k = -0.0177$ s/m) with that obtained by Mutschlecner and Whitaker ($k = 0.018$ s/m) using the SCI index show only a slight decrease in the magnitude of the correction, potentially attributable to using observed UKMO winds in place of the yearly average values. The difference in sign here is due to the definition of wind direction, that is, in meteorology wind direction is referenced to the direction it is coming from, though in reality the actual wind vector is pointed 180° from this direction. For example, a meteorologically stated westerly wind (270°) is describing physically a wind vector pointed eastward (90°). For this study we adopt the latter, more physical definition.

With the magnitudes of the wind corrections determined and combining Eqs. (16) and (20) the energy-infrasound regression equation, corrected for the presence of high-altitude winds, for bolides becomes

$$A = 10^{a-kv_h} R_S^b. \tag{22}$$

The final best-fit regression equations for the four measured signal properties, along with wind corrected values and error bounds are shown in Figs. 6a–h. By inverting these equations it becomes possible to solve for a bolide's yield directly from a given set of observations. Using Eq. (22) and the definition of scaled range (Eq. (14)) the yield equations have the form:

$$E_S = 10^{3(a-kv_h)/b} R^3 A^{-3/b}, \tag{23}$$

where E_S is the bolide's yield (initial kinetic energy) expressed in tons (2000 lbs) of equivalent TNT, R is the range to the bolide in kilometers, and a, b, k are the regression and wind correction constants given in Table 2 for the four bolide signal measurements.

To test the robustness of the combined satellite and infrasound relations for small bolide events, the

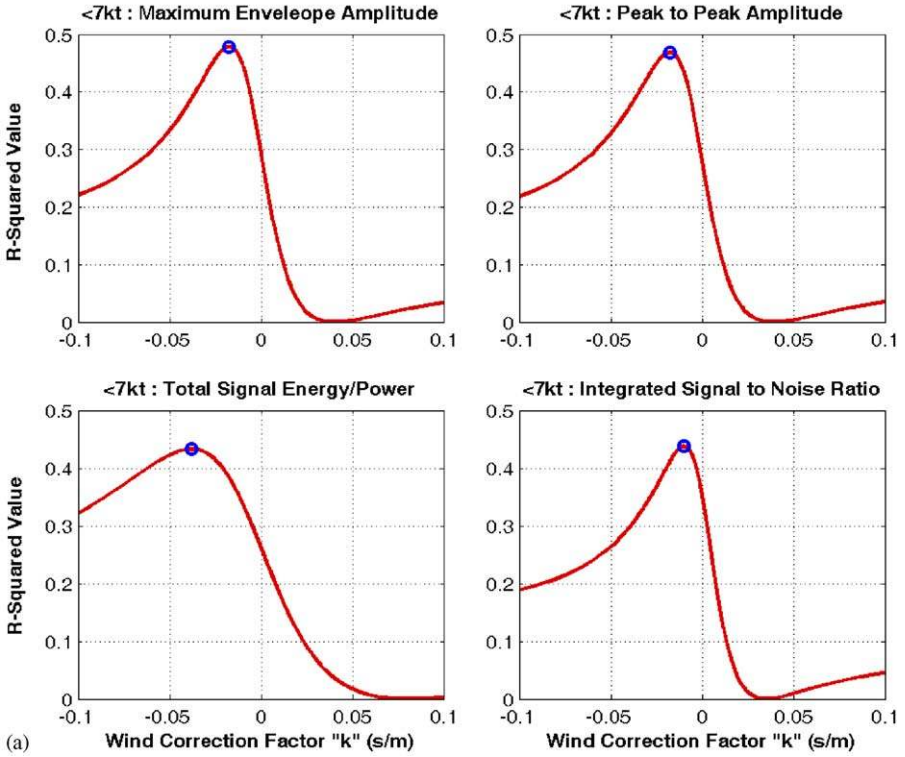

Fig. 5. Least-squares regression R^2 values as a function of the wind correction factor k for (a) small (<7 kt) and (b) large (>7 kt) bolides. In all cases correlation shows distinct peaks. For small bolides, these peaks are near similar values that have been found and used by previous authors (Table 2), while large bolides show k values near zero. This is attributed to observational biases in the observations of large events as described in the text.

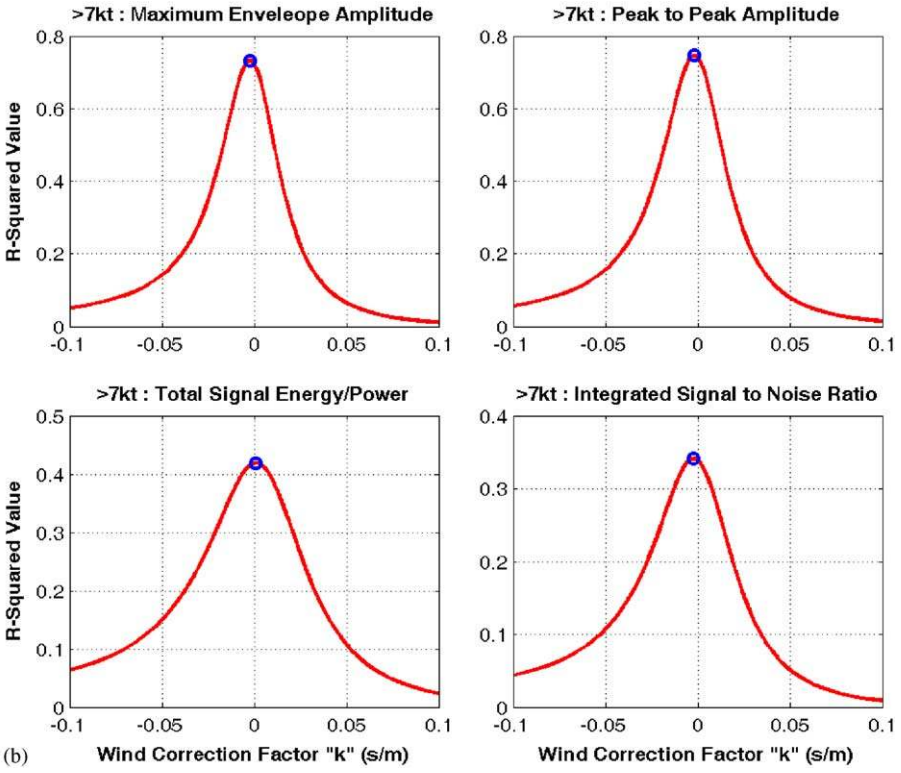

Fig. 5. (*Continued*)

infrasound observations with well-determined energies are plotted together with the measured yield calibration curves (Figs. 7a–d). These events include infrasound observations of the recent Villalbeto de la Peña, Park Forest, Neuschwanstein and Moràvka fireballs and use the same signal methodology discussed in the previous section. Appropriate scaled ranges for these measurements were determined using the initial mass and velocity estimates, determined from analysis of either video, photographic, radiometric, radionuclide or other independent observations of the individual fireballs/recovered meteorites (see Table 1 as given earlier for measurement details), rather then using the luminous efficiency method of Eqs. (10) and (11). In all cases, the infrasound observations plot within the 95% confidence interval of the satellite-infrasound observations and confirm that satellite determined energies and locations are consistent with equivalent ground-based measurements. Only in the case of the total integrated signal energy does there appear to be notable deviation from the regression curve; however, of all the measured quantities in our study integrated energy also shows the greatest variation. Conversely the integrated SNR shows the best correlation between satellite and ground-based infrasound observations; this emphasizes the importance of taking into account the noise floor at a particular infrasound station to make accurate source energy estimates. This consistency, coupled with the slightly smaller effect of high-altitude winds, makes this particular signal property the most robust bolide energy estimator. More generally, this indicates that well determined ground-based camera and infrasound observations of fireballs that provide ground truth in the form of meteorites should be used to refine and calibrate the satellite–infrasound relation from Brown et al. (2002a) in the future as more such events become recorded.

Finally, analysis of the remaining scatter about the newly wind corrected data for the small bolide population demonstrates the variability associated with applying a wind correction of the type adopted here. If all the small bolide infrasound observations are forced to lie upon their respective regression curves, the required wind magnitude value used in the wind correction would need to be adjusted (increased/decreased) by an average of: 21.8 m/s for maximum signal envelope amplitude, 21.2 m/s for

peak-to-peak amplitude, 22.6 m/s for integrated signal energy and 32.4 m/s for the integrated signal-to-noise ratio. These adjustments are comparable to the variation in the measured UKMO wind speeds seen along most propagation paths at stratospheric heights. Thus it may be reasonable to expect that some, if not most, of the remaining scatter is due to the variation in the wind field experienced by the wavefront along a particular propagation path, which is lost when expressed as a single average wind value. If this is a reasonable assumption, then a more detailed wind correction applied in the future could reveal more systematic changes in the bolide infrasound curves due to other non-wind related effects.

7. Comparison to nuclear and high explosive tests

Detection and characterization of explosive events in the atmosphere is one of the primary goals of the IMS network of infrasound arrays (Christie et al., 2001). While CTBT is most concerned with explosions pertaining to nuclear tests and enforcement of the Comprehensive Nuclear Test Ban Treaty, the

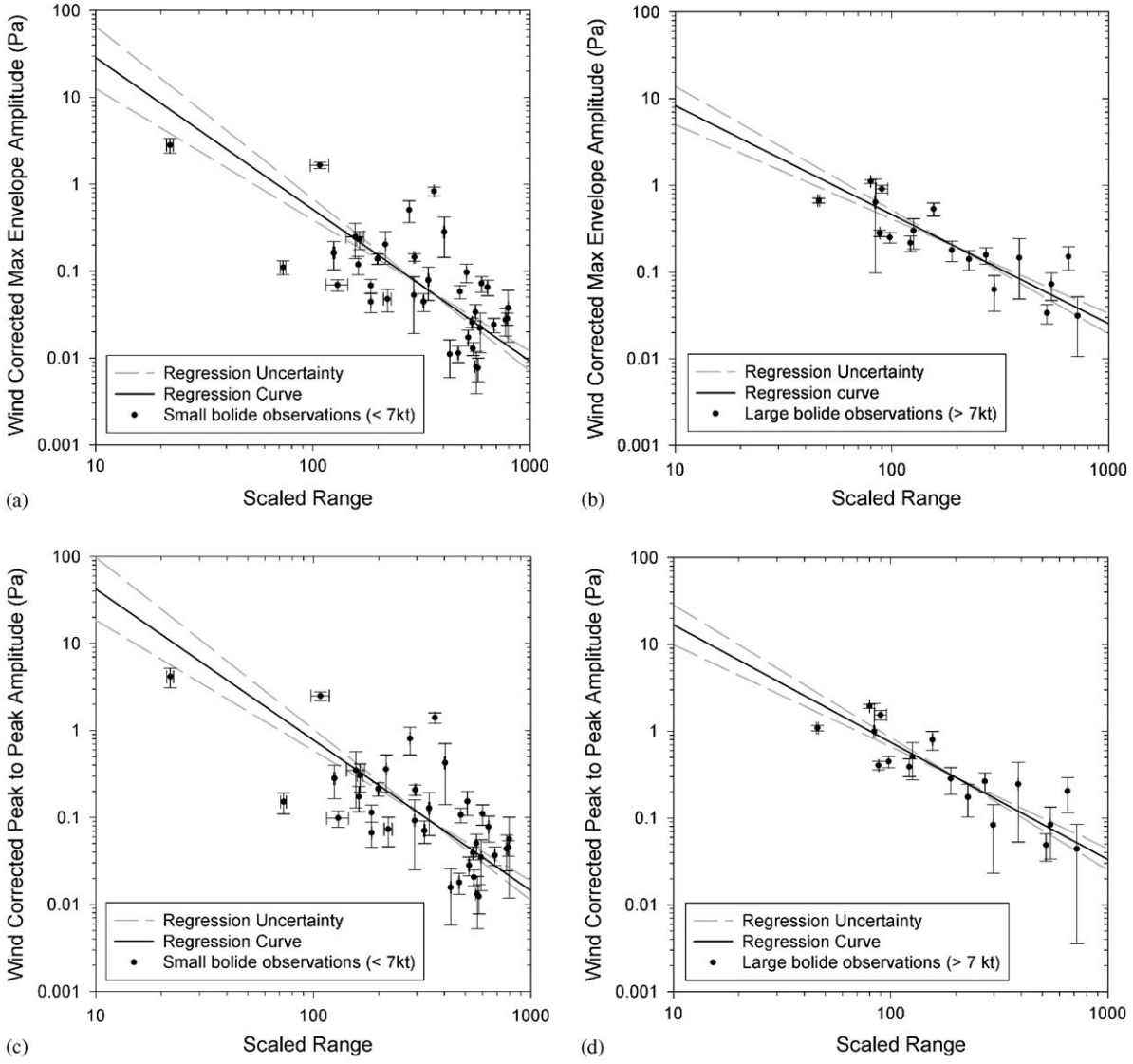

Fig. 6. Stratospheric wind corrected regression curves for small/large bolide infrasound measurements (a)/(b) maximum amplitude of signal envelope, (c)/(d) peak-to-peak amplitude, (e)/(f) total integrated signal energy, (g)/(h) integrated signal-to-noise ratio. After wind correction, in all cases, the fitted functions show decreased scatter and improved correlation.

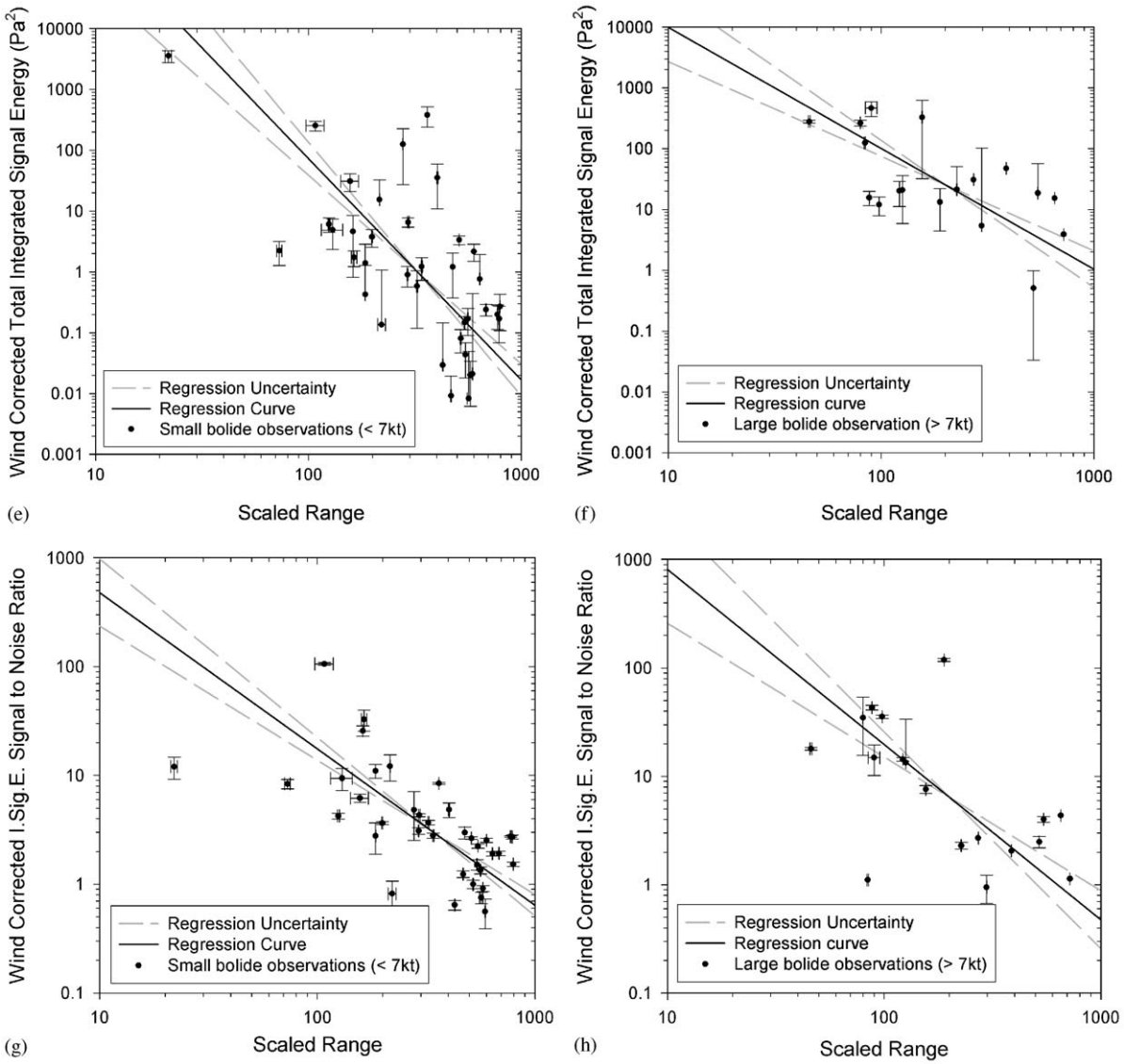

Fig. 6. (*Continued*)

Table 2
Regression and UKMO wind correction constants for bolide infrasonic signal measurements (see text for more details)

Signal property	k (s/m)	a	b
Max. sig. env. ampl. (<7 kt)	−0.0174	3.21±0.59	−1.75±0.24
Peak-to-peak ampl. (<7 kt)	−0.0177	3.36±0.60	−1.74±0.24
Tot. Int. Sig. Energy (<7 kt)	−0.0380	9.2±1.3	−3.64±0.53
Int. SNR (<7 kt)	−0.0100	4.12±0.51	−1.44±0.20
Max. sig. env. ampl. (>7 kt)	−0.0024	2.18±0.39	−1.26±0.17
Peak-to-peak ampl. (>7 kt)	−0.0018	2.58±0.41	−1.35±0.18
Tot. Int. Sig. Energy (>7 kt)	+0.0010	5.98±0.99	−1.99±0.43
Int. SNR (>7 kt)	−0.0023	4.53±0.88	−1.62±0.38

observation and interpretation of bolide airwaves worldwide can provide an efficient means of both testing this network and eventually allowing the signals to be efficiently differentiated from actual nuclear explosions (Chyba et al., 1998). Historical infrasonic observations of above-ground (free-air) nuclear and high yield chemical explosive tests (of known yields and locations) provide an effective means of comparison to these more recent bolide observations.

The method most commonly used in the past to determine the energy of an airborne explosion

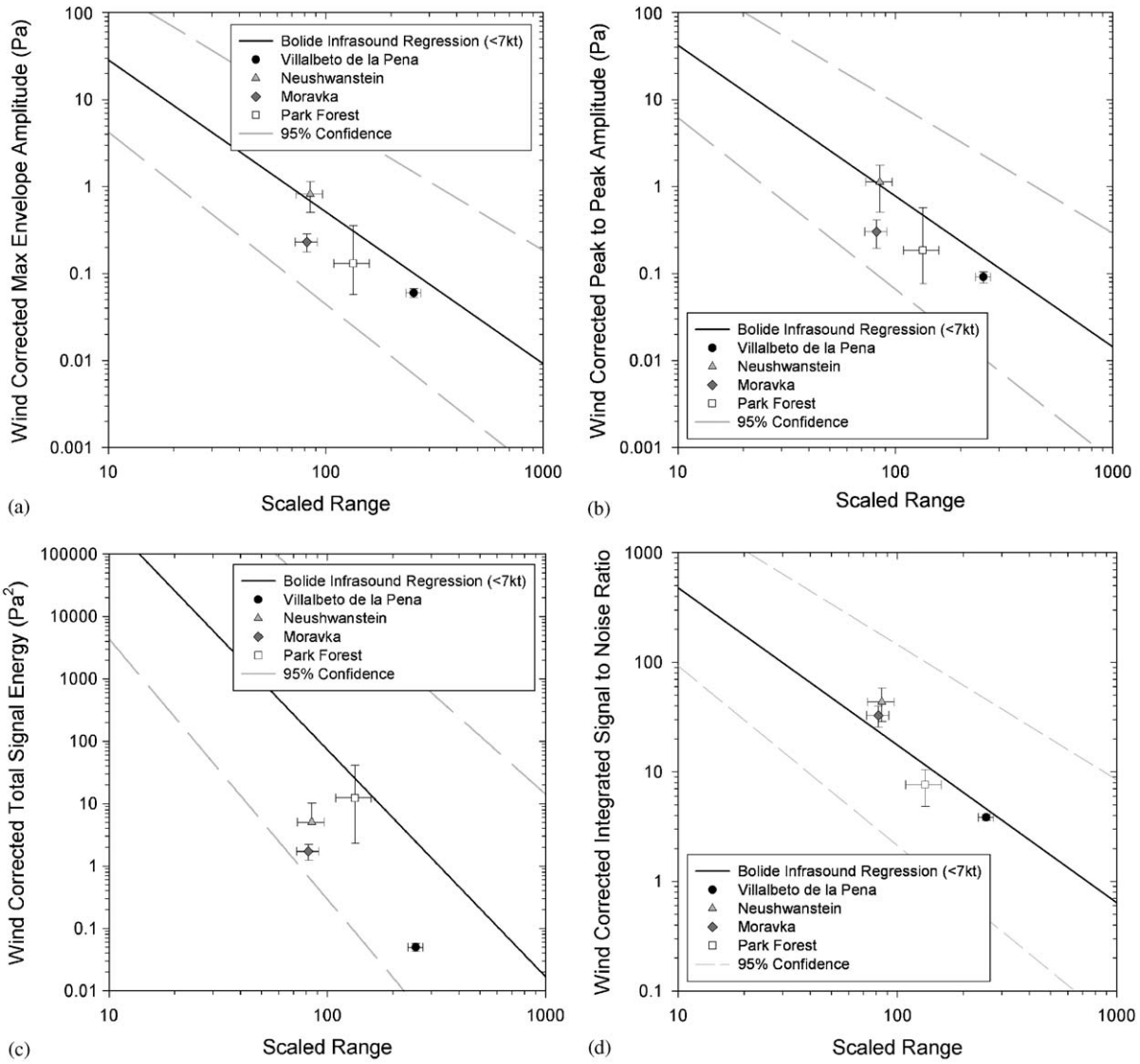

Fig. 7. Small bolide infrasound observations with well-determined, ground-based measurements of the initial kinetic energies in comparison to the general bolide infrasound regressions. (a) Maximum amplitude of signal envelope, (b) peak-to-peak amplitude, (c) total integrated signal energy, (d) integrated signal-to-noise ratio. In all cases, these well-determined observations plot well within the formal 95% confidence margins of the empirical energy relations. A particularly good regression fit is found for the integrated signal-to-noise measurement.

source (such as a bolide) from acoustic signals is the AFTAC empirical equations. These relate a signal's period at maximum amplitude to the yield of the explosion (Eqs. (5a) and (5b)). Unfortunately, these relations were derived using sources much larger than typical bolide energies, and as a result the AFTAC relations tend to break down at small source energies. To illustrate this effect, the source energies obtained using the AFTAC period relation (Eq. (5a)) and the measured periods for each bolide in our study are plotted against the satellite derived energies in Fig. 8. Here it can be seen that scatter increases both below ~0.2 kt as well as above 2 kt, with the tightest fitting region (and thus best source energy estimates) lying between these regimes. In addition, to the large amount of scatter at small energies, the shift produced by the wind on the signal period (Beer, 1974) is clearly seen when these periods are separated into with wind and counter wind observations (Fig. 9). Counter wind observations are preferentially observed at slightly longer periods and so produce larger energy estimates,

while the opposite is seen for downwind observations. The result is that the true period of the signal becomes obscured and the scatter along the AFTAC period relation increases, making the resulting energy estimates relatively poor when applied to such small yields.

Also noted in Fig. 9, is the increasingly poor AFTAC energy estimates for events with satellite energies >7 kt where observed periods are systematically larger. These large periods we suspect may be due to fragmentation of the meteoroid during its passage through the atmosphere. As a large bolide fragments, this fragment "cloud" may create a virtual blast cavity where shocks produced by several bodies traveling together merge to form a larger blast radius, and hence fundamental period, than would be the case for a single body. These larger periods are then systematically interpreted by the AFTAC period/energy relation as due to much larger source energies, by orders of magnitude. In these cases, amplitudes should be a more robust measure of the source energy as they are linked to the energy deposition along the meteor trail and not to the physical size of the blast cavity.

Comparison of the small bolide peak-to-peak amplitude curve to standard American National Standards Institute (ANSI) overpressure–distance curves (American National Standards Institute, 1983) for a 1 kt nuclear explosion (NE) and an 1134 kg (2500 lb) high yield chemical explosion (HE) (Reed, 1977), show distinct differences in both amplitude and slope (Fig. 10a). Observed bolide airwave pressures are consistently lower and drop off more rapidly with distance than those of either nuclear or chemical explosions. A similar comparison with the large bolide peak-to-peak amplitude curve (Fig. 10b) also shows this consistently lower observed pressure; however, for large bolides the slope of the regression curve is identical, within uncertainty, to the NE and HE curves. This led to a suspicion that the lack of observations below 100 in scaled range for small bolides had caused those few to act as pivot points during regression. To test this, the solitary observation below 50 in scaled range (Fig. 6c) was removed and the small bolide data regressed again. No significant change in slope was observed, thus it appears that the change in the slope between <7 kt and >7 kt events may indeed be real. Unfortunately events with energies from 1 to 6 kt observed at close ranges (less then 1000 km) are not very common and it may be some time before more observations are made and this can be confidently confirmed.

Although the cause of the apparent change in slope between the two-bolide curves is not well

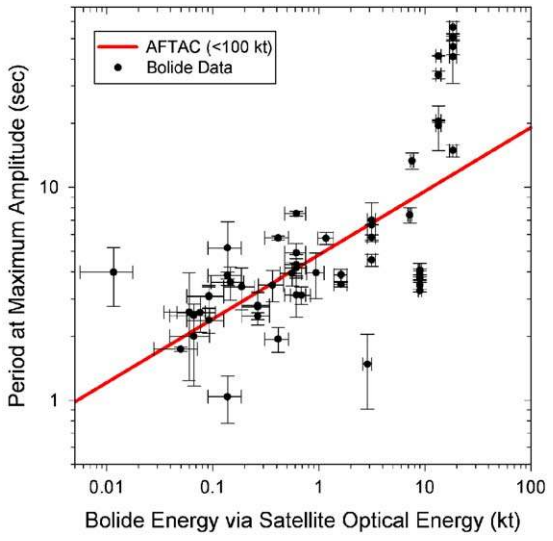

Fig. 8. Observed period at maximum amplitude for both small and large bolide signals as a function of satellite-deduced source energy. For comparison the commonly used AFTAC period–energy relation (Eq. (5a)), derived from nuclear test observations, is also shown.

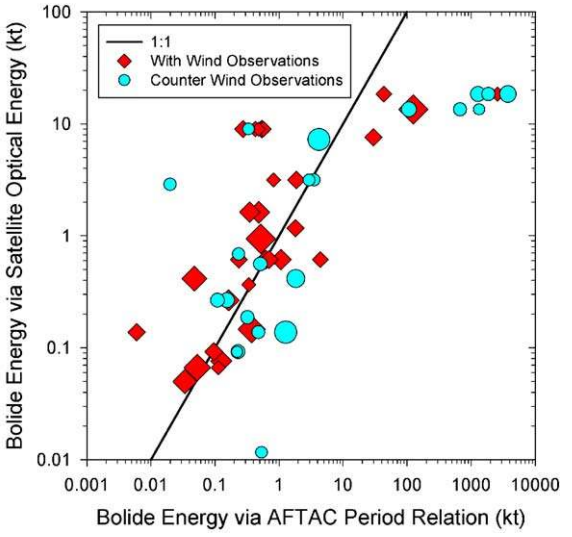

Fig. 9. Comparison of satellite optically derived energies to that of the AFTAC period–energy relation. Sizable differences exist between the two techniques. The period relationship potentially suffers from both doppler shifting of the true period by high-altitude winds resulting in a much broader range of deduced energies and overestimation of periods caused by fragmentation of larger meteoroids. *Note*: Increased sizes of individual points indicate the magnitude of the wind experienced for that observation.

understood, several physical reasons may exist to help explain the discrepancy in observed signal pressure. Despite the fact that the standard NE and HE curves in Figs. 10a/b are for free-air explosions, the altitude of these tests did not exceed a few kilometres above the ground surface. In comparison, typical terminal bolide detonations occur at altitudes of 20–40 km, depending greatly on the objects physical structure and velocity (Ceplecha et al., 1998). This difference in source altitudes requires that the ambient pressure at the bolide heights be ~5–0.3% of that of the near surface (United States Committee on Extension to the Standard Atmosphere, 1976). As a result, explosive overpressures produced at altitude will always produce higher observed pressures at the surface,

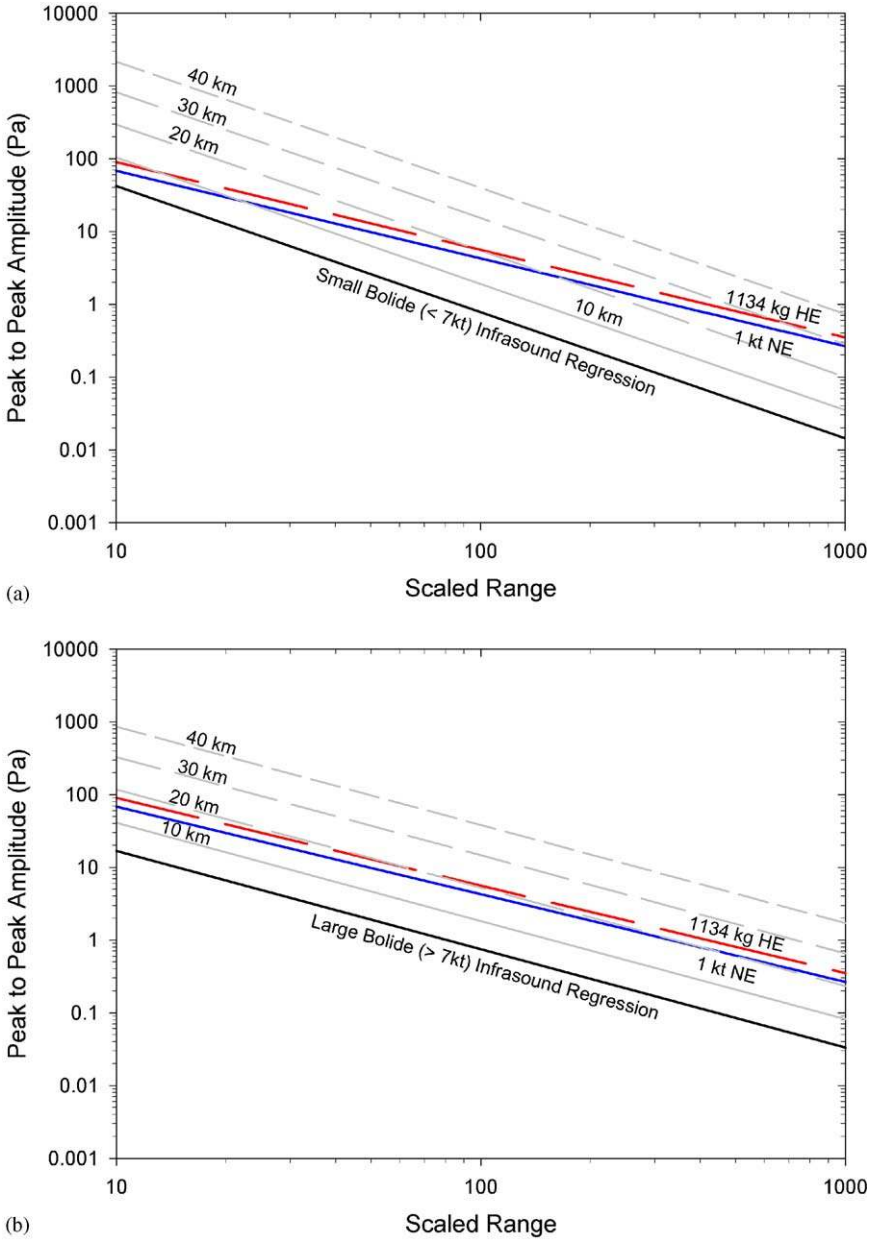

Fig. 10. Comparison of infrasonically observed bolides to ANSI standard 1 kt nuclear and 2500 lb (1134 kg) high explosive free-air explosion data for both (a) small and (b) large bolides. Gray lines indicate the resulting shift in the observed bolide regression if corrections for various source altitudes are included.

but lower overpressures ($\Delta p/p$) as the blast wave must conserve energy while propagating downward into the denser, higher pressure regions of the lower atmosphere.

This source altitude effect has been ignored in the observed bolide infrasound regression curves (Eq. (22)), due to unknown individual terminal detonation altitudes for most of the observed bolides; however, a correction for this effect does exist in Eq. (13). In the linear regime, the overpressure is proportional the ratio of source and ground pressures as (p_o/p) to the negative 2/3 power; scaling all values upward to match what would be observed if the source was located at the surface. Applying this correction to both the small and large bolide population curves for a series of source altitudes, an estimate for the average detonation altitude for 0.1 to 1 m diameter and 1–10 m class bolides, respectively can be made. These source altitude shifts are shown in gray in Fig. 10a/b for 10–40 km source altitudes. Observing where the source altitude shifted bolide curves cross the nuclear/chemical explosion line, a value of between 20 and 30 km altitude is determined for the average acoustic source altitude for the small bolide (<7 kt) infrasound data, consistent with the altitude range determined previously by Edwards et al. (2005) and in good agreement with independent observational data for fireballs and bolides in these size ranges (cf. Halliday et al., 1989). For the large bolide data, however, an altitude of ~20 km is found. This smaller source altitude correction result conforms to the physically expected result that large bolides should penetrate deeper into the atmosphere, and is consistent physically with the survivability of some material from 1 to 10 m class meteoroids (cf. Bland and Artemieva, 2003).

In addition to source altitude, another potential cause for the discrepancy between the bolide and man-made explosion curves may lie in the type of propagation the airwave undergoes before reaching the point of observation at the ground. Previously we have assumed that all propagation is essentially linear along the entire propagation path, though we know this is not strictly true. A more realistic model would be an initially nonlinear shock in the vicinity of the bolide, which after some distance will decay to a weakly nonlinear shock wave that eventually (after some unknown distance) transitions into a linearly propagating acoustic wave. It is during the second weakly nonlinear stage of this model, where attenuation of the overpressure is more rapid, decaying at the rate of

$$D_{WS}x^{-3/4}. \tag{24}$$

As compared to the linear case, which decays at the slower rate of

$$D_{L}x^{-1/2}, \tag{25}$$

where D_{WS} and D_{L} are the associated damping functions for weak shock and linear propagation, respectively and x is the distance from the source in units of blast radii (ReVelle, 1976). Here the blast radius for a meteor hypersonic shock (approximated as a cylindrical line source) is

$$R_0 \approx 1.05Md_m, \tag{26}$$

where R_0 is the blast radius, M is the mach number and d_m is the meteoroid diameter (ReVelle, 1976). The overall effect of the nonlinear-to-linear treatment is to cause observed pressures to be somewhat lower than is the case for the strictly linear treatment. The combination of bolide sources occurring at higher altitudes and our selection of long distance, stratospherically ducted airwave observations should ensure that weakly nonlinear shocks will propagate for longer distances before the transition to a linear acoustic wave occurs. However, precisely how far airwaves propagate nonlinearly through stratospheric waveguides, and thus how poor the linear approach approximation is, remains a matter of some speculation and is not easily definable quantitatively for bolide events in our study. Thus we acknowledge that although nonlinearity of the airwaves may affect the structure of the empirical relations, it is difficult to determine the magnitude of this effect on the observations without further work on the duration of the nonlinear signal propagation at stratospheric altitudes.

8. Comparison to theoretical models

Next we compare these empirical relations to theoretical treatments of initial bolide source energy. Fig. 11 shows source energy estimates from the two best correlated empirical small bolide relationships (peak-to-peak amplitude and integrated signal-to-noise ratio) compared to similar estimates using line source theory (Eq. (2)) which makes use of the measured signal periods. In most cases, several parameters remain unknown for bolide events in the data set; in these instances estimated mean values are used, however, on

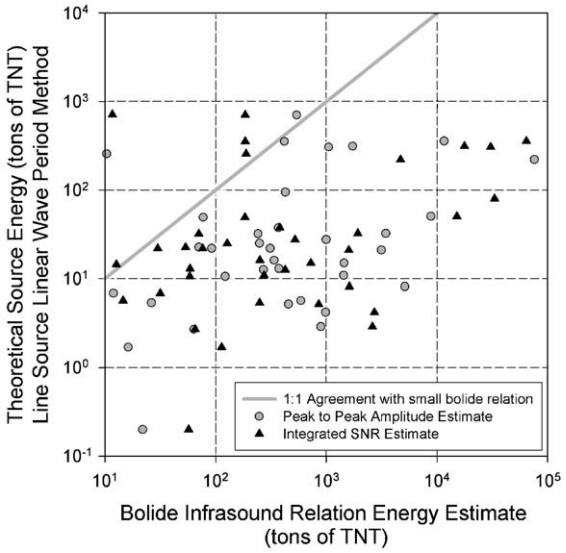

Fig. 11. Comparisons between theoretical and empirical source energy predictions for bolide infrasound using the small bolide peak-to-peak amplitude and integrated signal-to-noise ratio relationships.

physical grounds the actual values are expected to typically vary by no more than factors of 2 or 3. These parameters (together with their assumed average values) are: meteoroid bulk density (3400 kg/m^3), meteoroid velocity (20 km/s) (Bottke et al., 2003) and acoustic velocity (0.300 km/s). Also among this list of unknowns is the source altitude. Since the source altitude has a rather broad range, with any particular case depending on initial meteoroid velocity, mass and composition this prevents meaningful comparison of our empirical energy estimates with energy estimates using the weak shock model (Eq. (1)). This is a direct consequence of the fireball end height range typically varying from 20 to 40 km. As such the source altitude pressure (p_z) will vary more than an order of magnitude over this range, or roughly three atmospheric scale heights. Despite this shortcoming, for the case of the linear wave method for line sources (Eq. (2)), the theoretical energy estimates appear to be in moderate agreement with both empirical methods for lower yield events (Fig. 11), with progressively poorer agreement as the yield increases. Although outliers in the empirical relations (Figs. 6c/g) produce estimates >10 kt, the linear wave method for line sources systematically underestimates the source energy for long distance infrasonic observations of bolides. This is likely the result of exceeding the limits to which Eq. (2) applies, as at long ranges >1000 km the distance from the source will be far greater then the length of a meteoroid's trajectory. This is substantiated in part by a trend of increasing differences between estimates and observational range. As well, errors in the period measurement, potentially due to meteoroid fragmentation effects or caustics, will lead to large changes in source energy due to the large period dependence (fourth power) in Eq. (2). Thus for long range infrasonic observations of bolides there appear to be few options with regards to methods of source energy estimation; the best approach seems to be use of the new relations presented here and/or the nuclear weapons based relationships between period or amplitude and energy (Eqs. (5)–(9)).

9. Application to historical bolide infrasound observations

One of the important applications of these new calibrations is re-examination of historical fireballs where infrasonic observations were made and where uncertainty remains about the energy of the bolide. Three particular cases were chosen, due to the availability of acoustic measurements and prior attempts to estimate source energies. They are (1) The Kincardine Fireball—September 17, 1966, (2) The Revelstoke meteorite fall—March 31, 1965 and (3) the August 3, 1963 bolide located off the southeastern coast of the South African Prince Edward Islands. One deficiency in analyzing such events is a lack of upper atmospheric data. Here we make use of the average of computed UKMO wind estimates, for the day in question, between 1992 (first complete year of UARS satellite observations) to the present along the individual great circle propagation paths for each observation. Though not specific to the particular year and day of the event, this provides a mean expected wind value and a measure of its variability. A complete listing of the infrasonic measurements and wind estimates used is provided in Table 3.

Using these values, and the maximum signal envelope amplitude relation as a proxy for peak amplitude measurements, we find that the Kincardine fireball may have had an energy between 0.76 and 1.60 kt, for the range of wind conditions between lightly pro-wind and moderately counter wind, with a "nominal" energy of 1.10 kt. For comparison ReVelle (1976) estimated that this fireball had an equivalent line-source energy of

Table 3
Historical bolide infrasound observations and wind estimates

Location	Latitude	Longitude	Range (km)	Observed amplitude (Pa)	UKMO wind estimate (m/s)
Kincardine Fireball (44.2°N, 81.6°W): September 17, 1966					
Boulder, Colorado	40.0395	−105.2258	2270	0.125[a]	−0.8 ± 5.4
Revelstoke meteorite fall (49°N, 117°W): April 1, 1965					
Boulder, Colorado	40.0395	−105.2258	1550	0.80[b]	15.3 ± 11.8
Prince edward islands meteor event (51°S, 24°E): August 3, 1963					
			11730	0.18[a]	0.1 ± 4.7
			14317	0.19[a]	1.6 ± 3.9

[a]Amplitude measured zero to peak.
[b]Amplitude measured peak to trough.

~3e10 J/km, this is a surprisingly small value considering infrasound was observed more then 2200 km distant. ReVelle (1974) notes that this initial energy estimate is poor considering most of the energy was likely deposited in the final terminal burst and could be significantly larger. This new kinetic energy estimate appears to confirm this suspicion. A similar estimate using the peak-to-peak amplitude relation was performed for the Revelstoke meteorite fall resulting in an energy range of 0.61–3.20 kt with a nominal energy of 1.40 kt, which is in good agreement with recent energy estimates for Revelstoke of 0.24–2.4 kt (ReVelle, 1995). This is much smaller than early 20–70 kt energy estimates (Krinov, 1966; ReVelle, 1976) still often quoted in the literature.

Finally the largest by far of the three historical events examined here is the bolide that was observed infrasonically by US Air Force microbarometers to be located just off the coast of the Prince Edward Islands of South Africa in August 1963 (ReVelle, 1997). The previous energy estimate by ReVelle (1997), using the AFTAC period–energy relationship, estimates the energy of this event to be 1.1 Mt (1100 kt) of TNT equivalent energy, making it the largest bolide event yet recorded infrasonically since the Great Siberian Meteor in 1908. Using this historical event (along with others) ReVelle estimated the flux of NEOs within the 0.2–1100 kt energy range, however this rate is contrary to extrapolated later estimates by Brown et al. (2002a) using satellite observations, such that the infrasound data suggest the impact rate by larger bodies/energies (~1 Mt) are more frequent by a factor of 5 than extrapolation of the satellite data indicate. Thus the question has arisen whether the 1963 bolide was as large as originally estimated. Using the measurements of the Air Force data provided by ReVelle (1997) and the large bolide regression curve for the maximum signal envelope, energy estimates were made using the two stations which observed the event, noting that similar to the more recent large events >7 kt, UKMO wind estimates determine these observations were probably also made when wind conditions were light (<10 m/s) along the propagation paths. Estimated energies using the maximum amplitude of the signal envelope relation from closest station determines this event to be between 175 and 186 kt, while the further station estimates it to be between 338 and 375 kt. Averaging these estimates the large bolide regression curves provide an estimate of 266 ± 90 kt of TNT for the 1963 Prince Edward Islands event. This estimate, less then a third that of the previous estimate, brings the NEO influx curve of ReVelle (1997) into much better agreement with that provided by extrapolation of the satellite influx rate (Brown et al., 2002a).

10. Conclusions

Through the use of available simultaneous infrasonic and optical satellite observations of bolides, a series of empirically derived equations have been found that relate observational range, total initial energy and several readily measurable infrasound signal properties from typical stratospheric arrivals. These measured quantities include; the maximum amplitude of the signal envelope, peak-to-peak amplitude, total integrated energy (or power) of the signal and the integrated energy/power signal-to-noise ratio. These relations are an update/alternative to those introduced by Edwards et al.

(2005) as they include data previously unavailable, particularly for large yield events.

Using a correction for signal modification by stratospheric winds similar to that used by previous authors incorporating measured UKMO wind data, rather then the SCI index or modeled winds, it is found that similar wind correction factor magnitudes used for nuclear and conventional explosive infrasound also produce R^2 maxima when applied to "small" bolide data (source energies <7 kt). Wind corrections for "large" bolide data (energies >7 kt) are slight, likely due the low to moderate winds experienced along most of the propagation paths for these events in our data set. As a self-consistency check that these corrections make physical sense and are not just a statistical convenience, it is found for the small bolide data that the wind correction factor for integrated signal energy/power is nearly twice that of the independently measured signal amplitudes. This is exactly the behavior that would be expected for the relationship between acoustic amplitude and energy.

Comparison of the peak-to-peak amplitude relations to those of the standard free-air nuclear and chemical high explosive data indicate that bolide infrasound is consistently observed with lower amplitudes and, for small bolide events, is more highly attenuated. This apparent difference in the slopes of the small and large bolide data set suggests that there may be some mechanism occurring between source energies of 3–7 kt that causes larger source energies to attenuate more slowly and/or biases in the observation of these large events at long ranges.

Differences in the magnitude of observed signal pressures from bolides are attributed primarily to the higher source altitudes than their equivalent man-made near-surface explosive data and some unknown amount of nonlinear propagation. Correction for the higher source altitudes places the average bolide detonation altitude between 20 and 30 kilometres for small events (<7 kt) and at $\sim$20 km altitude for events (>7 kt). These altitudes are in good agreement with typical terminal altitudes determined through more conventional investigations for 0.1–1 m class meteoroids and are consistent with the expectation that larger 1–10 m class bodies should survive to lower altitudes (cf. Ceplecha et al., 1998). Quantifying the correction to acoustic amplitudes associated with nonlinear propagation is left for future work.

Further comparisons of observed bolide signal periods to the commonly used AFTAC energy–period relationships, derived from nuclear test data, show that at the very smallest source energies, scatter about the AFTAC curve correspondingly increases. This scatter can be attributed to the generally smaller source energies of typical bolides as compared to that of the nuclear tests used to develop the AFTAC relationship, in addition to the doppler shift of the observed period by high-altitude winds. Indeed, were it not for this effect, the period-energy relationship would likely improve significantly. However, it is not clear how to easily correct the observed period for this wind-induced doppler shift without significant computational efforts and complete global models of the atmospheric wind present at the time of individual events. Thus for bolides, in its uncorrected current state, the AFTAC period energy relation after regression demonstrates no better correlation ($R^2 = 0.478$) then most of the other infrasonic signal properties examined. As well, there is a consistent overestimation in source energy (in some cases by several orders of magnitude) between satellite derived energies and the energies derived from the AFTAC period relationship when applied to the largest events (>7 kt) in our database. We suggest that this is an effect of large-scale fragmentation of these more massive meteoroids in the atmosphere and subsequent creation of an artificially large collective blast cavity producing longer fundamental wave periods. Despite these limitations and potential biases, the AFTAC period relation does seem to be a reasonable means of estimating energies for events in the 0.1—a few kt range.

Acknowledgements

The author's extend thanks to Catherine Woodgold and David McCormack for their assistance in acquiring some of the recent bolide infrasound data used in this study and for helpful discussions. The British Atmospheric Data Centre provided access to UKMO weather data. PGB acknowledges Natural Resources Canada, the Canada Research Chair Program and the Natural Sciences and Engineering Research Council for funding support.

References

American National Standards Institute, 1983. Airblast Characteristics for Single Point Explosions in Air, ANSI Standard S2.20-1983. Acoustical Society of America, New York.

Astapowitsch, I.S., 1933. New data about the fall of the great meteorite on June 30, 1908, in central Siberia. Astronomical Journal of the Soviet Union 10, 465–483 (in Russian).

Astapowitsch, I.S., 1934. Air waves caused by the fall of the meteorite on 30th June, 1908, in Central Siberia. Quarterly Journal of the Royal Meteorological Society 60, 493–504.

Beer, T., 1974. Atmospheric Waves. Halsted Press, New York, USA.

Blanc, E., Millies-Lacroix, J.C., Issartel, J.P., Perez, S., 1997. Detection of nuclear explosions in the atmosphere. Chocs 17, 23–34.

Bland, P.A., Artemieva, N.A., 2003. Efficient disruption of small asteroids by Earth's atmosphere. Nature 424, 288–291.

Borovička, J., Spurný, P., Kalenda, P., Tagiaferri, E., 2003. The Morávka meteorite fall: 1. Description of the events and determination of the fireball trajectory and orbit from video records. Meteoritics and Planetary Science 38, 975–987.

Bottke, W.F., Vokrouhlicky, D., Rubincam, D.P., Broz, M., 2003. The effect of Yarkovsky thermal forces on the dynamical evolution of asteroids and meteoroids. In: Asteroids III. University of Arizona Press Tucson, AZ, pp. 395–408.

Brown, P., Hildebrand, A.R., Green, W.E., Page, D., Jacobs, C., ReVelle, D., Tagliaferri, E., Wacker, J., Wetmiller, B., 1996. The fall of the St-Robert meteorite. Meteoritics and Planetary Science 31, 502–517.

Brown, P., Spalding, R.E., ReVelle, D.O., Tagliaferri, E., Worden, S.P., 2002a. The flux of small near-Earth objects colliding with the Earth. Nature 420, 314–316.

Brown, P.G., Whitaker, R.W., ReVelle, D.O., Tagliaferri, E., 2002b. Multi-station infrasonic observations of two bolides: signal interpretation and implications for monitoring of atmospheric explosions. Geophysical Research Letters 29.

Brown, P.G., ReVelle, D.O., Tagliaferri, E., Hildebrand, A.R., 2002c. An entry model for the Tagish Lake fireball using seismic, satellite and infrasound records. Meteoritics and Planetary Science 37, 661–675.

Brown, P.G., Pack, D.W., Edwards, W.N., ReVelle, D.O., Yoo, B.B., Spalding, R.E., Tagliaferri, E., 2004. The orbit, entry dynamics and initial mass of the Park Forest Meteorite. Meteoritics and Planetary Science 29, 1605–1625.

Ceplecha, Z., Borovička, J., Elford, W.G., ReVelle, D.O., Hawkes, R.L., Porubčan, V., Šimek, M., 1998. Meteor phenomena and bodies. Space Science Reviews 84, 327–471.

Christie, D.R., Vivas Veloso, J.A., Campus, P., Bell, M., Hoffmann, T., Langlois, A., Martysevich, P., Demirovic, E., Carvalho, J., 2001. Detection of atmospheric nuclear explosions: the infrasound component of the International Monitoring System. Kerntechnik 66, 96–101.

Chyba, C.F., van der Vink, G.E., Hennet, C.B., 1998. Monitoring the Comprehensive Test Ban Treaty: possible ambiguities due to meteorite impacts. Geophysical Research Letters 25, 191–194.

Clauter, D.A., Blandford, R.R., 1998. Capability modeling of the proposed International Monitoring System 60-Station Infrasonic Network, LAUR-98-56, Los Alamos National Labs Report, Los Alamos, NM.

Cox, E.G., 1958. Sound Propagation in Air, Handbuch der Physik, vol. 48. Springer, Berlin, pp. 455–478.

Davidson, M., and Whitaker, R.W., 1992. Miser's Gold, LA-12074-MS, Los Alamos National Laboratory Report, pp. 1–28.

Dziewonski, A., Hales, A., 1972. Methods in Computational Physics, vol. 11. Academic Press, New York, pp. 39–84.

Edwards, W.N., Brown, P.G., ReVelle, D.O., 2005. Bolide energy estimates from infrasonic measurements. Earth, Moon and Planets, doi:10.1007/s11038-005-2244-4.

Evers, L.G., Haak, H.W., 2003. Tracing a meteoric trajectory with infrasound. Geophysical Research Letters 30, 1.

Glasstone, S., 1964. The Effects of Nuclear Weapons. United States Atomic Energy Commission, Washington, DC, USA.

Glasstone, S., Dolan, P.J., 1977. The Effects of Nuclear Weapons. United States Department of Defense and Department of Energy, Washington, DC, USA.

Golitsyn, G.S., Grigor'yev, G.I., Dokuchayev, V.P., 1977. Generation of acoustic-gravity waves by meteor motion in the atmosphere. Izvestiya 13, 633–639.

Halliday, I., Blackwell, A.T., Griffin, A.A., 1989. The typical meteorite event, based on photographic records of 44 fireballs. Meteoritics 24, 65–72.

Harris, J.M., Young, C.J., 1997. MatSeis; a seismic graphical user interface and toolbox for MATLAB. Seismological Research Letters 68, 307–308.

Hedin, A.E., Fleming, E.L., Manson, A.H., Schmidlin, F.J., Avery, S.K., Clark, R.R., Franke, S.J., Fraser, G.J., Tsuda, T., Vial, F., Vincent, R.A., 1996. Empirical wind model for the upper, middle and lower atmosphere. Journal of Atmospheric and Terrestrial Physics 58, 1421–1447.

Klekociuk, A.R., Brown, P.G., Pack, D.W., ReVelle, D.O., Edwards, W.N., Spalding, R.E., Tagliaferri, E., Bernard, Y.B., Zagari, J., 2005. Lidar, satellite and acoustic measurements of an asteroidal airburst in Earth's atmosphere. Nature 436, 1132–1135.

Krinov, E.L., 1966. Giant Meteorites. Pergamon Press, Oxford, New York, USA.

Llorca, J., Trigo-Rodríguez, J.M., Ortiz, J.L., Docobo, J.A., García-Guinea, J., Castro-Tirado, A.J., Rubin, A.E., Eugster, O., Edwards, W.N., Laubenstein, M., Casanova, I., 2005. The Villalbeto de la Peña Meteorite Fall: I. Fireball energy, meteorite recovery, strewn field and petrography. Meteoritics and Planetary Science 40, 795–804.

Melton, B.S., Bailey, L.F., 1957. Multiple signal correlators. Geophysics 22, 565–588.

Mutschlecner, J.P., Whitaker, R.W., 1990. The correction of infrasound signals for upper atmospheric winds, NASA, Langley Research Center. Proceedings of the Fourth International Symposium on Long-Range Sound Propagation, pp. 143–153.

Reed, J.W., 1977. Attenuation of explosion waves. Journal of the Acoustical Society of America 61, 39–47.

ReVelle, D.O., 1974. Acoustics of meteors—effects of the atmospheric temperature and wind structure on the sounds produced by meteors. Ph.D. Dissertation, University of Michigan, Ann Arbor, MI.

ReVelle, D.O., 1976. On meteor-generated infrasound. Journal of Geophysical Research 81, 1217–1229.

ReVelle, D.O., 1995. The fall of the Revelstoke meteorite: March 31, 1965: seismic and infrasonic analyses of the impact location of the meteorites and search for catering features, *LAUR-95-1952*, pp. 1–2.

ReVelle, D.O., 1997. Historical detection of atmospheric impacts by large bolides using acoustic-gravity waves. In: J.L. Remo (Ed.), Annals of the New York Academy of Sciences, Near-Earth Objects—The United Nations International

Conference, New York Academy of Sciences, vol. 822, pp. 284–302.

ReVelle, D.O., 2005. Recent Advances in bolide energy modeling: a bolide potpourri. Earth, Moon and Planets doi:10.1007/s11038-005-9064-4, 1–36.

ReVelle, D.O., Whitaker, R.W., 1995. Acoustic Efficiency Analysis using Infrasound from NEOS, *LAUR-95-4121,* Los Alamos National Laboratory Report, Los Alamos, New Mexico.

ReVelle, D.O. and Whitaker, R.W., 1997. Acoustic efficiency analysis using infrasound from NEOs. In: S.W. Johnson (Ed.), Proceedings of the Fifth International Conference of Space 96, Albuquerque, New Mexico.

ReVelle, D.O., Brown, P.G., Spurny, P., 2004. Entry dynamics and acoustics/infrasonic/seismic analysis for the Neuschwanstein meteorite fall. Meteoritics and Planetary Science 39, 1605–1626.

Shumilov, O.I., Kasatkina, E.A., Tereshchenko, E.D., Kulichkov, S.N., Vasil'ev, A.N., 2003. Journal of Experimental and Theoretical Physics Letters 77, 115–117.

Spurny, P., Oberst, J., Heinlein, D., 2003. Photographic observations of Neuschwanstein, a second meteorite from the orbit of the Příbram chondrite. Nature 423, 151–153.

Stevens, J.L., Adams, D.A., Baker, G.E., Xu, H., Murphy, J.R., Divnov, I. and Bourchik, V.N., 2002. Infrasound modeling using Soviet Explosion Data and Instrument Design Criteria from Experiments and Simulations. Proceedings of the 22nd Annual DoD/DoE Seismic Research Symposium, New Orleans, USA.

Swinbank, R., O'Neill, A.A., 1994. Stratosphere–Troposphere Data Assimilation System. Monthly Weather Review 122, 686–702.

Tagliaferri, E., Spalding, R., Jacobs, C., Worden, S.P., Erlich, A., 1994. Hazards Due to Comets and Impacts. University of Arizona Press, Tucson, AZ, p. 199.

United States Committee on Extension to the Standard Atmosphere, 1976. U.S. Standard Atmosphere 1976, U.S. Government Printing Office, Washington.

Webb, W.L., 1966. Structure of the Stratosphere and Mesosphere. Academic Press, New York, USA.

Whipple, F.J.W., 1930. The Great Siberian meteor and the waves, seismic and aerial, which it produced. Quarterly Journal of the Royal Meteorological Society 56, 287–304.

Whipple, F.J.W., 1934. On phenomena related to the great Siberian meteor. Quarterly Journal of the Royal Meteorological Society 60, 505–513.

Whitaker, R.W., 1995. Infrasonic monitoring, In: Proceedings of the 17th Seismic Research Symposium on Monitoring a Comprehensive Test Ban Treaty, pp. 997–1000.

Young, C.J., Chael, E.P., Merchant, B.J., 2002. Version 1.7 of MatSeis and the GNEM R&E regional seismic analysis tools. Proceedings of the 24th Seismic Research Review, pp. 915–924 (CD-ROM).